

Federated Deep Equilibrium Learning: A Compact Shared Representation for Edge Communication Efficiency

IEEE Publication Technology, *Staff, IEEE,*

Abstract—Federated Learning (FL) is a prominent distributed learning paradigm facilitating collaboration among nodes within an edge network to co-train a global model without centralizing data. By shifting computation to the network edge, FL offers robust and responsive edge-AI solutions and enhance privacy-preservation. However, deploying deep FL models within edge environments is often hindered by communication bottlenecks, data heterogeneity, and memory limitations. To address these challenges jointly, we introduce FeDEQ, a pioneering FL framework that effectively employs deep equilibrium learning and consensus optimization to exploit a compact shared data representation across edge nodes, allowing the derivation of personalized models specific to each node. We delve into a unique model structure composed of an equilibrium layer followed by traditional neural network layers. Here, the equilibrium layer functions as a global feature representation that edge nodes can adapt to personalize their local layers. Capitalizing on FeDEQ's compactness and representation power, we present a novel distributed algorithm rooted in the alternating direction method of multipliers (ADMM) consensus optimization and theoretically establish its convergence for smooth objectives. Experiments across various benchmarks demonstrate that FeDEQ achieves performance comparable to state-of-the-art personalized methods while employing models of up to 4 times smaller in communication size and 1.5 times lower memory footprint during training.

Index Terms—Federated Learning, Distributed Optimization, Equilibrium Models, Edge Networks.

I. INTRODUCTION

With the rapid proliferation of Internet-connected devices and the consequent vast data they generate, the shortcomings of centralized computing are becoming increasingly evident. Edge networks have emerged as a compelling countermeasure, processing data closer to its source. Such networks capably manage the escalating data volumes, inherently reducing latency, optimizing bandwidth usage and improving real-time responsiveness. In tandem with this shift towards decentralized processing, Federated Learning (FL) has been recognized as an apt machine learning paradigm for the network edge. Contrasting with traditional methods that necessitate transferring all data to a central server, FL enables multiple edge nodes to collaborate on training a unified machine learning model. Here, each node refines the model using its local data and transmits only the model's updates to a central server, where they are aggregated to improve the global model [1]. This not only aligns with privacy requirements since data never leaves

the network edge, but also provides scalable solutions tapping into the distributed processing power of edge devices.

Despite offering a scalable, privacy-preserving solution that taps into the distributed processing power of edge devices, fully realizing FL's potential within complex edge environments is contingent upon overcoming three major challenges. First, there are *communication bottlenecks*, resulting from the need to transmit large model parameters between parties. These constraints can lead to significant bandwidth limitations, causing inefficiencies and delays in training. Second, *data heterogeneity* arises from the variety and diversity of the data held by edge nodes, leading to client drift effects where individual model performances diverge. Finally, *the limitations in memory and storage* constrain the complexity and size of the models that can be deployed, requiring innovative solutions to maximize the potential of FL in edge network scenarios.

Recent literature has presented diverse approaches to address the foregoing challenges, as outlined in Fig. 1. The communication and memory challenges has been tackled using model compression techniques [2, 3] to reduce model size for facilitating transmission and adaptive gradients [4] for efficient parameter updates. On the other hand, personalization has emerged as a key strategy to address the issue of data heterogeneity and client drift. Full model personalization methods, such as meta-learning [5, 6] and multi-task learning [7–9], have shown efficiency in capturing unique local patterns. However, these techniques can be resource-intensive and may necessitate considerable communication overhead. Conversely, partial model personalization approaches [10, 11] offer a balanced solution by employing a shared representation complemented by personalized local models, enabling both customization and conservation of resources. While these methods typically tackle individual challenges, a comprehensive approach that can addressing both communication and memory constraints, as well as data heterogeneity within FL in edge networks remains yet to be thoroughly explored in research.

In this paper, we address a pivotal question: "*How do we leverage FL to exploit a compact shared representation under data heterogeneity in edge networks that not only substantially reduces communication bandwidth and memory footprint but effectively enhance learning performance?*". To this end, we propose a novel framework, namely *Federated Deep Equilibrium Learning* (FeDEQ), that leverages consensus optimization to learn a shared representation via deep equilibrium models (DEQs), combined with personalized explicit layers for each edge node. The compact shared layer

This paper was produced by the IEEE Publication Technology Group. They are in Piscataway, NJ.

Manuscript received April 19, 2021; revised August 16, 2021.

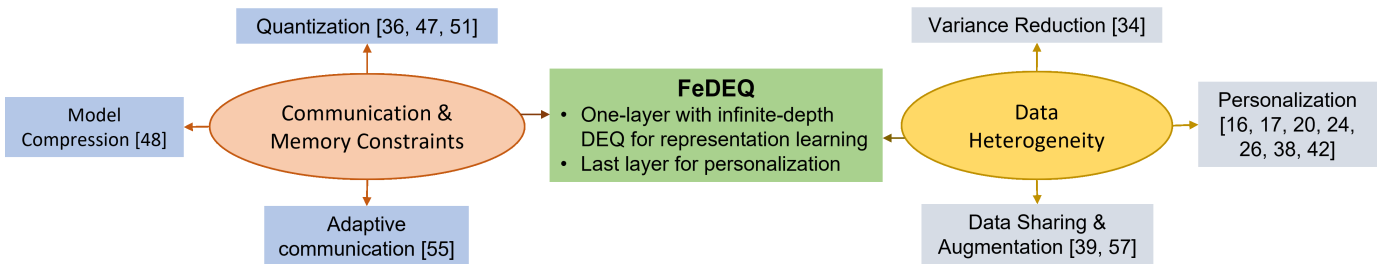


Fig. 1: FeDEQ aims to simultaneously address data heterogeneity and communication and resource constraints, while other methods focus on solving individual challenge.

can capture diverse patterns across edge nodes, while the explicit layers are fine-tuned for personalization using local data. This combination enables us to effectively handle the aforementioned challenges: FeDEQ performs on par with state-of-the-art (SOTA) approaches while reducing communication by 2–4 times and memory footprint by 1.5 times. The main contributions of this work are summarized as follows.

- We introduce FeDEQ, a novel framework tailored for resource-efficient and personalized FL under data heterogeneity in edge networks. Central to FeDEQ’s design is its ability to learn a *compact shared representation* with constant memory footprint via equilibrium models, thereby adapting this shared base to swiftly fine-tune *personalized layers* at individual edge node to achieve local personalization.
- To collaboratively learn shared and personalized layers across edge nodes, we devise a consensus optimization scheme grounded in the alternating directions method of multipliers (ADMM). This strategically decomposes the original consensus problem into the primal problem – seeking optimal personalized and shared parameters, and the dual problem – controlling discrepancies between the local and shared representation to mitigate the drifting effect in local training.
- We theoretically provide the convergence guarantees for the proposed algorithm for smooth objectives. Under mild assumptions, we show that FeDEQ converges to a stationary point, which achieves a shared representation across all edge nodes and optimal personalized parameters for each node.
- Through extensive experimentation on several FL benchmarks, we substantiate that FeDEQ achieves personalization with communication and memory efficiency. Further, the shared layer is highly adaptable to new edge nodes in generalization experiments.

To the best of our knowledge, this is the first work that employs deep equilibrium learning and ADMM consensus optimization for simultaneously tackling communication bottlenecks, memory constraints and data heterogeneity in FL for edge networks.

II. RELATED WORK

A. Federated learning at the Network Edge.

The emergence of FL comes in response to three significant challenges in large-scale machine learning, particularly parti-

ent to edge networks: processing massive amounts of edge data, managing the heavy communication load within networks, and preserving privacy without resorting to centralized storage. The standard federated algorithm - FedAvg [1], which utilizes local stochastic gradient descent (SGD) and averaging, has established the foundational framework for much of the FL research in edge networks.

The primary challenges of FL in the context of edge networks can be broadly classified into communication and resource bottlenecks and data heterogeneity. *Communication and memory bottlenecks* pertain to the large number of model parameters that need to be exchanged and large models that need to be trained on edge nodes. These challenges have prompted prior works to create more communication and computation-efficient strategies including: quantization [12–14], where local computations reduce the precision of model updates to reduce the size of data transferred; model compression [2], which involves reducing the size of the model to make it more manageable to transmit; and adaptive communication [4], where the amount of data exchanged is adjusted dynamically based on various factors like network conditions.

The second category, *data heterogeneity*, is concerned with the non-identically distributed (non-i.i.d.) data that are often present across edge nodes. This aspect of the data can affect the convergence and performance of the global model [15], leading to a variety of approaches to mitigate its impact. Studies have delved into methods for managing the diversity of data across edge nodes, incorporating techniques like data sharing [16], data augmentation [17] or variance reduction [18] to recognize and adapt to the variations in data across different nodes in the network, ensuring that the globally aggregated model accurately reflects the underlying patterns of the entire distributed dataset.

B. Personalized Federated Learning

Personalized Federated Learning (PFL) has recently gained significant attention to address data heterogeneity [19]. Regarding full model personalization, a simple yet effective personalization approach involves fine-tuning the global model’s parameters for each client [20, 21]. Various works adopted multi-task learning (MTL), enabling clients to learn their distinct data patterns while benefiting knowledge shared by others [7–9]. Meta-learning frameworks are also employed to develop an effective initial model to rapidly adapted to new heterogeneous tasks [5, 6], while model interpolation techniques are used to personalize models using a mixture of

global and local models [22, 23]. Recent years, partial model personalization approaches [10, 11, 24–29] have brought up the idea of exploiting the common representation in heterogeneous settings to learn a personalized model tailored for each device, enabling simple formulation and layer-wise flexibility; however, their applicability is limited to specific settings such as linear representations [10] or pre-trained representations [28].

C. Deep Equilibrium Learning

Equilibrium models has emerged as a fascinating topic in the realm of implicit deep learning in recent times. In contrast to the conventional layer stacking models, deep equilibrium models (DEQ) implicitly define layers through an equilibrium point (a.k.a. fixed-point) of an infinite sequence of computation [30]. A general DEQ consists of a single implicit layer f_θ modeled as a fixed-point system $z^* = f_\theta(z^*; x)$. Here, θ is the model parameter, x is the input data, and the equilibrium z^* is approximated by fixed-point iterations or root-finding. Several works [31, 32] delved into the theoretical underpinnings of DEQ, providing valuable insights into the stability and approximation properties of implicit layers. Recent works have successfully applied DEQ on large-scale tasks such as sequential modeling, and semantic segmentation [30, 33]. Despite potential drawbacks such as slow training time and computational complexity, DEQ possesses the capability to mitigate communication overhead and memory-intensive deep models, thereby presenting a compelling solution for FL.

D. ADMM-based learning

ADMM has made significant advancements in both theory and application over recent decades, particularly in distributed learning [34–36]. In FL, several ADMM-based decentralized methods have been developed to enhance communication efficiency [37, 38]. However, employing this framework for tackling data heterogeneity is still uncharted.

In this work, we also inherit the ideas of partial personalization that efficiently learn non-linear representations with a reduced model size using only edge local data.

III. PROBLEM FORMULATION

A. Federated Deep Equilibrium Learning

Consider a federated learning setting within an edge network consisting of a central server and n edge nodes. Each node i owns a dataset of n_i independent and identically distributed (i.i.d.) observations, denoted as $\{(x_{ij}, y_{ij}) \in \mathcal{X}_i \times \mathcal{Y}_i : j = 1, \dots, n_i\}$. This local dataset represents a crucial piece of the learning puzzle, capturing unique patterns and characteristics inherent to each specific node’s region or domain. To distill meaningful insights from this data, we introduce a predictive function $f_i : \mathcal{X}_i \rightarrow \mathcal{Y}_i$, tailored to the unique statistical properties of each node’s local data, and a loss function $\ell(f_i(x_{ij}), y_{ij})$ measuring the discrepancy between $f_i(x_{ij})$ and y_{ij} . The local empirical risk on node i , defined as $\mathcal{L}_i = \frac{1}{n_i} \sum_{j=1}^{n_i} \ell(f_i(x_{ij}), y_{ij})$, reflects how well the model is performing within the individual local context. The primary

objective is to minimize the global risk, equal to the sum of all local risks.

Conventional FL approaches, such as FedAvg [1], learn a global model by averaging the model parameters obtained from edge nodes after local SGD rounds. While this method promotes collaboration among nodes, it ignores the intricacy of heterogeneous data which leads to suboptimal performance. A prominent way to rectify this drawback is through the implementation of partial personalization, where a model decouples into a *representation module* and a *personalized module*. The former serves as a collaborative learning ground for edge nodes to acquire a common representation (either linear or non-linear) that captures the shared patterns and regularities across all nodes’ data. This common learning phase helps maintain a unified and consistent model view. On the other hand, the *personalized module* adapts and refines itself to the unique characteristics of each node’s local data, thereby enabling better local generalization [10, 24, 28].

While this personalization approach offers a more nuanced handling of the data and can lead to improved model performance, it is not without challenges. An effective representation is typically deep and complex, often consisting of numerous parameters and layers - as illustrated by the representation r in Fig. 2a, which includes M layers. This complexity translates into substantial communication costs and $O(M)$ memory complexity during training. These costs can prove to be significant barriers, particularly in resource-constrained edge networks where efficiency is paramount.

In this work, we concurrently tackle these challenges of data heterogeneity, communication overhead, and memory constraints by leveraging partial personalization and model compactness through the utilization of deep equilibrium, as shown in Fig. 1. Specifically, for every node i we consider a special predictive function f_i of the form

$$\begin{aligned} f_{\theta_i, w_i}(x_{ij}) &:= h_{w_i}(g_{\theta_i}(z_{ij}^*; x_{ij})) \\ \text{s.t. } z_{ij}^* &= g_{\theta_i}(z_{ij}^*; x_{ij}), \quad \forall i, j. \end{aligned} \quad (1)$$

By this definition, f_i is a composite of two functions: g parametrized by θ_i and h by w_i . A schematic illustration is presented in Fig. 2b. While h_{w_i} can be any conventional layer (or stack of layers), such as a fully-connected network, g_{θ_i} is defined implicitly with the constraint $z_{ij}^* = g_{\theta_i}(z_{ij}^*; x_{ij})$. Such a representation for g_{θ_i} is called a *deep equilibrium model* [30], and the key advantage lies in its compactness and expressive power: a single layer can represent an infinitely deep weighted network while maintaining a constant memory footprint [30]. This allows the model to learn a sophisticated non-linear representation at a low memory capacity. We describe this in detail in Sec. III-B below.

We then formulate a global consensus optimization problem for FeDEQ as follows:

$$\begin{aligned} \min_{\{\theta_i\}, \{w_i\}, \theta} \quad & \sum_{i=1}^n \left[\mathcal{L}_i(\theta_i, w_i) := \frac{1}{n_i} \sum_{j=1}^{n_i} \ell(f_{\theta_i, w_i}(x_{ij}), y_{ij}) \right] \\ \text{s.t. } \quad & \theta_i = \theta, \quad \forall i. \end{aligned} \quad (2)$$

This mathematical representation embodies a critical balance

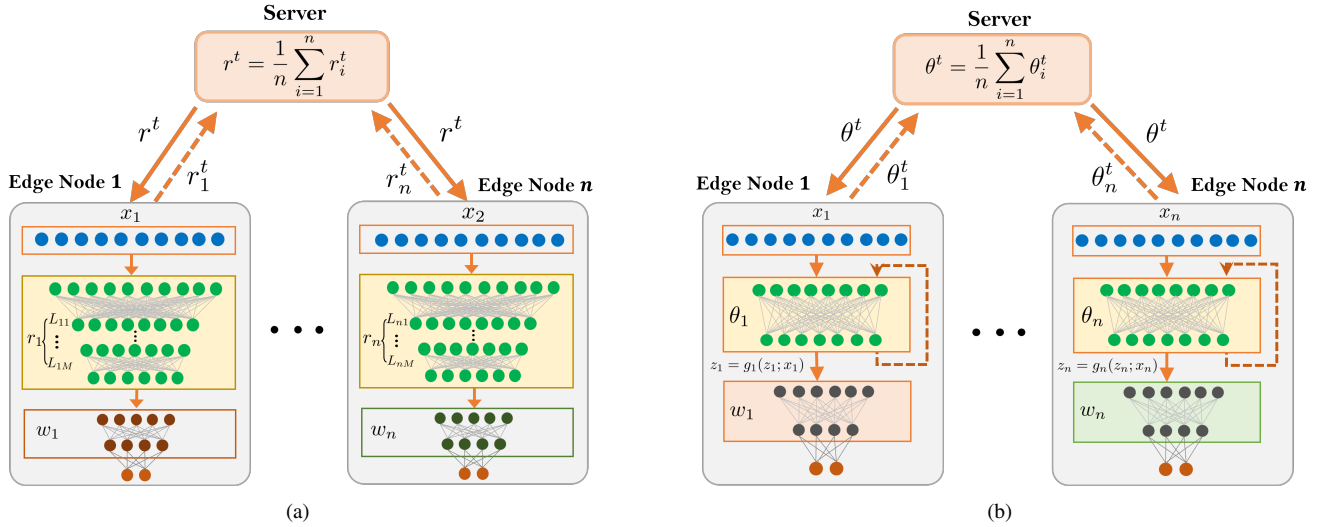


Fig. 2: Using explicit and implicit layers as a shared representation module for edge nodes in FL. (a) Each node has M explicit layers in its model. (b) Instead of having multiple explicit layers, each node uses only one equilibrium layer parametrized by θ_i .

between global coherence and local customization. The consensus constraints $\theta_i = \theta, \forall i$ are to enforce that the local θ_i are learned through sharing among edge nodes. This encourages the representation layer to benefit from the structure of all nodes' data—the objective of FL. On the other hand, all w_i are fine-tuned locally, adapting from the shared representation to achieve personalization. In Sec. IV below, we present a novel algorithm to solve this optimization problem based on ADMM consensus optimization.

B. Equilibrium Layers: Forward Pass and Backward Pass

A single equilibrium layer in the constraint of (1) embodies an “infinitely deep” network through a fixed-point system. Here we examine a common non-linear mapping of the form:

$$z = g_\theta(z; x) := \phi(Bz + Cx + b), \quad (3)$$

where $x \in \mathbb{R}^d$ is the input, $z \in \mathbb{R}^{d_1}$ is the output, $\theta = (B \in \mathbb{R}^{d_1 \times d_1}, C \in \mathbb{R}^{d_1 \times d}, b \in \mathbb{R}^{d_1})$ is the parameters and $\phi: \mathbb{R}^{d_1} \rightarrow \mathbb{R}^{d_1}$ is some nonlinear activation functions. Equation (3) implies that z^* is a fixed point of the function $z \mapsto \phi(Bz + Cx + b)$ for a given data point (or a mini-batch) x : an equilibrium layer of the form (3) is equivalent to feeding the input through an infinite sequence of weight-tied layers of a feedforward network. It has been observed that such a single layer, while much smaller in size, can perform on par with deep networks containing many explicit layers. This makes implicit representations particularly appealing for FL since the communication of model parameters is often a bottleneck.

1) *Forward Pass – Fixed-Point Representation:* In the general problem (1) or the special case (3), we aim to find an equilibrium state z^* such that $z^* = g_\theta(z^*; x)$, where g_θ is a neural network parameterized by θ and x is the input to the model. The fixed-point formulation allows a single equilibrium layer to capture long-range dependencies as all parts of the input contribute to the equilibrium state z^* . Moreover, in the process of finding z^* , the model implicitly emphasizes features

that are stable under g_θ , promoting robust and consistent representations. Additionally, if the input distribution changes, the DEQ can adapt by finding a new equilibrium, enabling dynamic adaptation to data changes. However, there remain two subproblems that affect the forward pass of DEQ optimization including fixed-point convergence and fixed-point solver.

Fixed-point convergence. From a theoretical perspective, a unique fixed point z^* offers an equilibrium representation under g_θ . The convergence of fixed-point iteration is strongly tied to the properties of the function g_θ , where a crucial condition for the guaranteed convergence is that g_θ needs to be a contraction mapping. This means that there exists a Lipschitz constant $L < 1$ such that $\|g_\theta(x) - g_\theta(y)\| \leq L\|x - y\|$ for all x, y in the domain of g_θ . If g_θ is a contraction mapping, the Banach fixed-point theorem guarantees the convergence to a unique fixed point [39]. However, ensuring that g_θ is a contraction mapping can be challenging in practice, given that g_θ is typically a deep neural network, capable of representing highly complex and non-linear functions.

Therefore, we make two assumptions following the theory in [31]. First, ϕ is a component-wise non-expansive (CONE) mapping, i.e., (i) the k th component of its output only depends on the k th component of its input and (ii) when operating on scalar input, ϕ is 1-Lipschitz continuous: $\forall u, v \in \mathbb{R}, |\phi(u) - \phi(v)| \leq |u - v|$. Many activation functions in deep learning, such as tanh, sigmoid, and (leaky) ReLU, satisfy this property. Second, the infinity norm of B , denoted by $\|B\|_\infty$, is strictly bounded above by 1. Together, these assumptions imply that g_θ in (3) is a contraction mapping, and a fixed point z^* exists for all input x . The use of l_∞ projection can promote fixed-point convergence in certain iterative methods by limiting the size of the updates. Specifically, after each update, the resulting point is “projected” onto a set defined by an ∞ -norm ball. For a matrix $B \in \mathbb{R}^{d_1 \times d_1}$ in (3) and radius $\kappa > 0$ we can employ l_∞ projection by solving the following problem.

$$\min_A \frac{1}{2} \|A - B\|_F^2 \quad \text{s.t.} \quad \|A\|_\infty \leq \kappa. \quad (4)$$

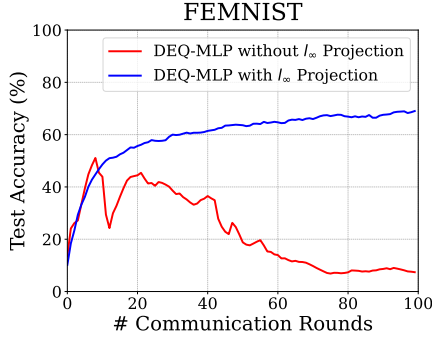


Fig. 3: FedAvg using DEQ-MLP with and without l_∞ projection

This problem can be solved by decomposing across rows and applying existing methods such as Bisection [31]. We demonstrate these findings to an FL context that involves 100 edge nodes, each possessing a portion of the FEMNIST dataset for a 62-class classification task. To benchmark, we employ the widely used FedAvg algorithm and compare two local model configurations: (i) a DEQ-MLP network with a single equilibrium layer of size 512 (DEQ-MLP), wherein the parameters associated with z are projected onto the l_∞ norm, succeeded by a linear layer of size 128, and ultimately, a final layer mapping to 62 classes; and (ii) a similar network architecture but without the projection step. As illustrated in Fig. 3, the DEQ-MLP network with the projection mechanism achieves convergence, whereas the network without projection appears to be diverging.

Fixed-point Solver. Recent works leverage Broyden [30, 40] and Anderson Acceleration (AA)[33, 41, 42] for solving fixed-point systems in DEQs. In this work, we employ a variant of AA to expedite the convergence of fixed-point iterations. The concept behind AA is to form the next iterate as a linear combination of past iterates, rather than merely relying on the last iterate. Specifically, AA minimizes the differences between the iterates and their mapped values over a history of m previous iterations. In terms of representation learning in FeDEQ, we suggest a warm-start strategy for AA in which the fixed point of the previous iterations is reused as the initial point for the next. Since the changes in θ and x are small from one iteration to the next (i.e., $\theta^{(i)} \approx \theta^{(i-1)}$ and $x^{(i)} \approx x^{(i-1)}$), the fixed points $z^{(i)}$ and $z^{(i-1)}$ are likely to be close to each other as well. This could bring several benefits:

- *Faster Convergence:* As the input data changes slightly from one iteration to the next, reusing the fixed point could lead to faster convergence of the fixed-point iteration, which could in turn speed up the overall training process.
- *Continuity of Representations:* The learned representations could exhibit a form of continuity or smoothness from one iteration to the next. This could potentially make the learned representations more robust and stable, especially in the face of small changes in the input data or the underlying function.
- *Improved Robustness:* If the model is trained on a stream of data that changes over time, reusing the fixed point could make the model more robust to these changes, as it provides a form of context from the previous data.

2) *Backward Pass – Implicit Differentiation:* Once the equilibrium state z^* has been found in the forward pass, the model computes the loss \mathcal{L} based on this state and the target output. The goal in the backward pass is to update the parameters θ to minimize this loss. The gradient of the loss \mathcal{L} w.r.t. θ is calculated by employing the chain-rule as follows:

$$\frac{\partial \mathcal{L}}{\partial \theta} = \frac{\partial \mathcal{L}}{\partial z^*} \frac{\partial z^*(\theta)}{\partial \theta} \quad (5)$$

In this context, the gradient of \mathcal{L} w.r.t. z^* can be derived through backpropagation. The notation $z^*(\theta)$ is also utilized to signify situations where z^* is perceived as an implicit function of the variables that we’re differentiating w.r.t. the shared parameter θ , and we use z^* on its own when we’re just mentioning the equilibrium value. Because of the self-consistent nature of the equilibrium state z^* , the gradient $\partial z^*(\theta)/\partial \theta$ cannot be computed directly. Instead, implicit differentiation is used. By differentiating the fixed-point equation $z^* = g_\theta(z^*; x)$ w.r.t. θ , we get:

$$\frac{\partial z^*(\theta)}{\partial \theta} = \frac{\partial g_\theta(z^*; x)}{\partial \theta} = \frac{\partial g_\theta(z^*; x)}{\partial z^*} \frac{\partial z^*(\theta)}{\partial \theta} + \frac{\partial g_\theta(z^*; x)}{\partial \theta} \quad (6)$$

Upon reorganizing the terms, we attain an explicit formulation for the Jacobian as follows.

$$\frac{\partial z^*(\theta)}{\partial \theta} = \left(I - \frac{\partial g_\theta(z^*; x)}{\partial z^*} \right)^{-1} \frac{\partial g_\theta(z^*; x)}{\partial \theta} \quad (7)$$

where I is the identity matrix, and $\frac{\partial g_\theta}{\partial z^*}$ and $\frac{\partial g_\theta}{\partial \theta}$ are the Jacobians of g_θ w.r.t. z^* and θ , respectively. Although the right-hand side terms can be explicitly computed using conventional automatic differentiation, solving the inverse of Jacobian is computationally intensive, especially when z^* is high-dimensional. To solve this equation more efficiently, we can employ the following vector-Jacobian product (VJP) [43].

$$y^T \left(\frac{\partial z^*(\theta)}{\partial \theta} \right) = y^T \left(I - \frac{\partial g(z^*; x)}{\partial z^*} \right)^{-1} \left(\frac{\partial g(z^*; x)}{\partial \theta} \right). \quad (8)$$

which is equivalent to the following linear system:

$$u^T = u^T \left(\frac{\partial g_\theta(z^*; x)}{\partial z^*} \right) + y^T. \quad (9)$$

where $u^T = y^T \left(I - \frac{\partial g_\theta(z^*; x)}{\partial z^*} \right)^{-1}$ is the solution of the linear system, which can be solved efficiently by using linear solvers such as conjugate gradient descent [44]. To this end, by substituting (7) to (5), we can have a form of VJP as follows.

$$\frac{\partial \mathcal{L}}{\partial \theta} = \frac{\partial \mathcal{L}}{\partial z^*} \left(I - \frac{\partial g(z^*; x)}{\partial z^*} \right)^{-1} \frac{\partial g(z^*; x)}{\partial \theta} \quad (10)$$

This can be solved using the above implicit differentiation techniques. The gradient $\partial \mathcal{L}$ is then used in gradient-based optimization methods to update the model parameters θ and minimize the loss.

One of the significant advantages of DEQs’ backward pass is their memory efficiency. In traditional deep learning models, the

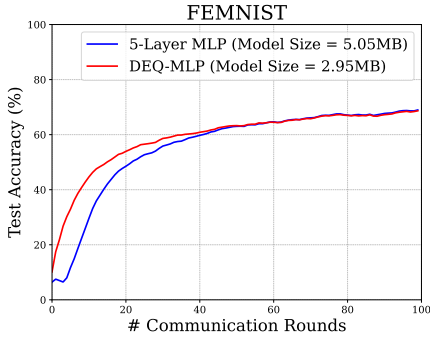


Fig. 4: FedAvg with 5-layer MLP model vs. DEQ-MLP

activations of all layers need to be stored for backpropagation. In contrast, DEQs only need to store the final equilibrium state, as all layers are the same and share the same parameters. This results in substantial memory savings, especially for very deep networks. Furthermore, DEQs allow for end-to-end training with gradient-based optimization methods [30]. Despite the complexity introduced by the fixed-point iteration and implicit differentiation, the backward pass is still differentiable, and gradients can be computed and used for parameter updates.

Jacobian-Free Backpropagation. The main challenge in the backward pass of DEQs is the extensive computational time, even though existing methods can avoid computing the inversion of a Jacobian matrix directly. Surprisingly, recent research has demonstrated implicit differentiation can be performed by using the zeroth-order approximation of the Neumann series for the inverse of the Jacobian matrix [45] instead of explicitly computing of this expensive term. This approach still provides satisfactory performance with significantly reducing computation time. Hence, in this work, we employ this Jacobian-Free backpropagation approach to estimate the implicit gradients.

C. Federated Learning with DEQs vs. Explicit Models

Previous work has shown that equilibrium layers can achieve similar performance to explicit layers while maintaining a compact model size [30]. We extend this finding to an FL context with 100 edge nodes, each holding a portion of the FEMNIST dataset for a 62-class classification task. We employ the de-facto FedAvg to compare two local model settings: (i) an MLP network with 4 explicit layers of size 512, followed by a linear layer of size 128, and a final layer mapping to 62 classes; and (ii) the same network with the four explicit layers replaced by a single equilibrium layer of size 512 (DEQ-MLP) as in (3). Fig. 4 shows that the same test accuracy is achieved in both settings. However, since setting (ii) requires a model that is 41% smaller in size, its communication cost is saved by nearly half per round. In Sec. V, we provide experiments with much more sophisticated models like DEQ-ResNet and DEQ-Transformer that also highlight this benefit.

IV. CONSENSUS OPTIMIZATION FOR FEDERATED LEARNING WITH EQUILIBRIUM LAYERS

With the objective (2), we introduce an ADMM consensus optimization variant to collaboratively learn the shared

parameters θ_i and the personalized parameters w_i . We detail the optimization procedure in Algorithm 1 and provide some remarks on its convergence at the end of this section.

A. Learning shared representation via ADMM Consensus Optimization

In FL for edge networks, the data heterogeneity across diverse edge nodes often culminates in a pronounced challenge known as *client drift* [18]. Such drift emerges when edge nodes, optimizing their model based on uniquely distributed data, converge toward a local objective minimum. This local convergence may differ considerably from the global optimization objective desired for an aggregated model. Consequently, when the server integrates models from myriad nodes, it often encounters a compounded effect of these varied local minima. The resulting global model, unfortunately, can become an aggregate that fails to optimally represent any individual edge node’s data, leading to overall suboptimal performance.

Motivation for using ADMM in Combatting Client Drift Effects. To mitigate the challenges posed by data heterogeneity and client drift, we have formulated the consensus optimization problem (2) to find a shared representation across all edge nodes and propose to employ ADMM [34] to solve it. This algorithm is based on alternating updates of primal and dual variables to achieve two goals: θ_i across edge nodes become closer and the objective function decreases. Applying this to our problem, we first introduce a dual variable λ_i for each θ_i and construct the following augmented Lagrangian for each client i :

$$\tilde{\mathcal{L}}_i(\theta, \theta_i, w_i, \lambda_i) := \mathcal{L}_i(\theta_i, w_i) + \langle \lambda_i, \theta_i - \theta \rangle + \frac{\rho}{2} \|\theta_i - \theta\|^2 \quad (11)$$

where $\rho > 0$ is the penalty parameter.

Upon solving the local augmented Lagrangian, clients will then collaboratively minimize the global objective $\tilde{\mathcal{L}}$, which is defined as follows.

$$\tilde{\mathcal{L}}(\theta, \{\theta_i\}, \{w_i\}, \{\lambda_i\}) := \sum_{i=1}^n \left[\tilde{\mathcal{L}}_i(\theta, \theta_i, w_i, \lambda_i) \right], \quad (12)$$

Delving deeper into the augmented Lagrangian (11), two essential terms come to the forefront. The inner product term, $\langle \lambda_i, \theta_i - \theta \rangle$, reflects the alignment between the deviation of a local model from the global model and its associated dual variable, λ_i . Essentially, it acts as a controller of discrepancies between local and global models. The quadratic term, $\frac{\rho}{2} \|\theta_i - \theta\|^2$, directly penalizes deviations of the local model from the global standard. The parameter ρ adjusts the stringency of this penalty, ensuring a balance between local adaptability and global consensus. These terms result in the new correction term in the gradient $\nabla_{\theta_i} \tilde{\mathcal{L}}_i = \nabla_{\theta_i} \mathcal{L}_i + \lambda_i + \rho(\theta_i - \theta)$ aligning client updates with server directions to overcome client drifts.

As described in detail in Algorithm 1, the ADMM consensus optimization proceeds by iteratively updating the local parameters θ_i and w_i , the dual variables λ_i , and the shared global parameters θ . This procedure consists of three key steps per communication round. First, the server performs averaging to update the shared parameters θ based on the set of θ_i obtained from the previous round (line 5) and then sends it to a new subset of edge nodes (line 7). Second, each selected node

i minimizes the augmented Lagrangian $\tilde{\mathcal{L}}_i$ w.r.t. the primal variables (lines 8–9). This local minimization makes use of the REP_UPDATE procedure (lines 13–20), which involves solving Problems (1) and (10) to obtain the gradient $\nabla_{\theta_i} \tilde{\mathcal{L}}_i$ via implicit differentiation. The dual variable λ_i is then updated by an ascent step to enforce the consensus constraint (lines 10–11). This process is repeated within a number of iterations until convergence, at which point the local representation θ_i and the consensus variable θ agree, resulting in a shared representation learned from the distributed data.

B. Personalization through Explicit Layers

With the shared representation θ learned via ADMM consensus optimization, we proceed to the second aim of FeDEQ, which focuses on achieving personalized model for each node to better address data heterogeneity. Particularly, in every communication round, node $i \in S$ fine-tunes its personalized parameters w_i on top of the shared representation θ with its local data, i.e., minimizing the original loss $\mathcal{L}_i(\theta, w_i)$ w.r.t. w_i (Line 8 of Algorithm 1). This problem can be efficiently solved by using traditional gradient-based optimization methods such as SGD, where the personalized parameter w_i^t obtained from the previous round t is used as the initial value for updating the next w_i^{t+1} , providing edge nodes the flexibility adapt to their unique data distributions to different personalization settings.

By decomposing the global problem into local subproblems and a consensus step, ADMM consensus procedure seeks a balance between local objectives and the global objective. The augmented Lagrangian (11) introduces a penalty for deviations from the consensus. Thus, even if a node’s local data pushes its model towards a distinct local minimum, the consensus penalty nudges it closer to the global consensus. Furthermore, with the penalty parameter ρ , ADMM can be adjusted in terms of how strictly it enforces consensus. This provides flexibility to tune the degree of consensus based on the extent of client drift observed.

Furthermore, combining equilibrium models with the ADMM consensus optimization framework enhances communication efficiency in key ways. Equilibrium models, with their implicitly “infinite-depth” single layer, simplify model complexity and reduce communication overhead by requiring fewer parameters. Moreover, they maintain a constant, often lower, memory footprint than traditional deep models, thus enabling resource-constrained edge devices to manage complex models without straining hardware resources. Additionally, the ADMM framework permits asynchronous updates of local parameters, thereby optimizing network resource utilization and convergence speed.

C. FeDEQ: Convergence Analysis

We present a theoretical analysis for FeDEQ’s convergence in a smooth, non-convex setting. In comparison with the original consensus optimization problem in [34, §7.1], our problem is different in four key aspects.

First, on edge node i the loss function \mathcal{L}_i is non-convex w.r.t. (θ_i, w_i) . Therefore, Algorithm 1 is based on a more recent treatment of ADMM for non-convex objectives in [46,

Algorithm 1 FeDEQ

- 1: **Parameters:** Communication rounds T ; penalty ρ
 - 2: Initialize $S_0 = \{1, \dots, n\}$, and $\theta^0 = \theta_i^0, w_i^0$ and λ_i^0 randomly for $i = 1, 2, \dots, n$
 - 3: **for** $t = 0, 1, \dots, T - 1$ **do** ▷ Global iteration
 - 4: Server aggregates the shared parameters:

$$\theta^{t+1} = \frac{1}{|S_t|} \sum_{i \in S_t} \theta_i^t$$
 - 5: Server randomly samples a subset S_{t+1} of edge nodes
 - 6: **for** each edge node $i \in S_{t+1}$ in parallel **do**
 - 7: Receive θ^{t+1} from server ▷ Communication
 Update primal variables:

$$\begin{cases} w_i^{t+1} \leftarrow \arg \min_{w_i} \mathcal{L}_i(\theta^{t+1}, w_i) \\ \theta_i^{t+1} \leftarrow \text{REP_UPDATE}(\tilde{\mathcal{L}}_i(\theta^{t+1}, \theta_i^t, w_i^{t+1}, \lambda_i^t)) \end{cases}$$
 - 8: $w_i^{t+1} \leftarrow \arg \min_{w_i} \mathcal{L}_i(\theta^{t+1}, w_i)$
 - 9: $\theta_i^{t+1} \leftarrow \text{REP_UPDATE}(\tilde{\mathcal{L}}_i(\theta^{t+1}, \theta_i^t, w_i^{t+1}, \lambda_i^t))$
 - 10: Update dual variable: $\lambda_i^{t+1} = \lambda_i^t + \rho(\theta_i^{t+1} - \theta^{t+1})$
 - 11: Send θ_i^{t+1} to server ▷ Communication
-
- 12: **function** REP_UPDATE($\tilde{\mathcal{L}}_i(\theta, \theta_i, w_i, \lambda_i)$)
 - 13: **Parameters:** local dataset $(\mathcal{X}_i, \mathcal{Y}_i)$, learning rate η
 - 14: **for** each local epoch **do**
 - 15: **for** each sample $(x, y) \in (\mathcal{X}_i, \mathcal{Y}_i)$ **do**
 - 16: Find the fixed-point $z^* = g_{\theta_i}(z^*; x)$
 - 17: Compute the loss $\mathcal{L}_i(h_{w_i}(g_{\theta_i}(z^*; x)), y)$
 - 18: Compute the gradient $\nabla_{\theta_i} \mathcal{L}_i$ using Eq. (10)
 - 19: Update gradients $\nabla_{\theta_i} \tilde{\mathcal{L}}_i = \nabla_{\theta_i} \mathcal{L}_i + \lambda_i + \rho(\theta_i - \theta)$
 - 20: Update: $\theta_i \leftarrow \theta_i - \eta \nabla_{\theta_i} \tilde{\mathcal{L}}_i$
 - return** θ_i
-

Algorithm 3]. In particular, we assume that \mathcal{L}_i is differentiable and L -Lipschitz smooth w.r.t. (θ_i, w_i) . Based on this, the update of these variables is done using gradient descent steps, which allows us to bound the decrease in $\tilde{\mathcal{L}}_i$ after lines 8–9. Further, the gradient w.r.t. w_i can be found via the traditional backward propagation procedure, as w_i is the parameter of an explicit module. On the other hand, the gradient w.r.t. θ_i , the parameters of an implicit module, is found using the implicit function theorem, which we have previously detailed in Sec. III-B.

Second, as is typical of FL algorithms, we must allow for node sampling, i.e., only a subset of edge nodes is required to participate in training in each global iteration t . This is done via choosing the subset S_{t+1} (line 5) and only aggregating the parameters θ_i from the sampled nodes (line 4). To assist the convergence analysis, we make an assumption that, regardless of the sampling method, there exists a period of $T > 0$ global rounds after which *all edge nodes* will have participated at least once. In [46], this is called the period- T essentially cyclic update rule.

Third, we employ *variable splitting* for our ADMM variant. In other words, the primal variable is split into θ_i and w_i on each node, and only θ_i is subject to the consensus constraint in (2). Moreover, unlike the original ADMM version which minimizes $\tilde{\mathcal{L}}_i$ jointly w.r.t. θ_i and w_i , we split the update of these variables in Algorithm 1. For w_i (line 8), since it is not constrained, minimizing the augmented Lagrangian is equivalent to minimizing the loss function \mathcal{L}_i . Then, θ_i is updated by minimizing $\tilde{\mathcal{L}}_i$.

Fourth and finally, as is common in large-scale machine learning, parameters are learned using optimization with *mini-*

batches. This gives us stochastic gradients w.r.t. the parameters θ_i and w_i , and as a result, the augmented Lagrangian is not guaranteed to decrease after every SGD round (it is only guaranteed in expectation).

We make the following assumption for our convergence analysis.

Assumption IV.1. For every node i , the local loss function \mathcal{L}_i is bounded below. Further, \mathcal{L}_i is differentiable everywhere w.r.t. (θ_i, w_i) and has Lipschitz gradients with parameter $L > 0$.

Remark IV.2. This assumption is common in deep learning's non-convex optimization analysis, ensuring gradient stability and the existence of an optimal solution.

To establish a convergence guarantee in a non-convex setting of ADMM, we aim to show the following. Start with the variables $(\theta^t, \{\theta_i^t\}, \{w_i^t\}, \{\lambda_i^t\})$. After T rounds (i.e., after all edge nodes have participated at least once since iteration t), the new variables $(\theta^{t+T}, \{\theta_i^{t+T}\}, \{w_i^{t+T}\}, \{\lambda_i^{t+T}\})$ lead to decrease in the global augmented Lagrangian $\tilde{\mathcal{L}}$. Then we show these variables will converge to a local stationary point of $\tilde{\mathcal{L}}$. The following result establishes the convergence of FeDEQ.

Lemma IV.3 (Decrease in augmented Lagrangian after every T iterations). *Suppose ρ is chosen large enough that $\rho > 6L$. After T global iterations since t , when all edge nodes have participated in training at least once, we have*

$$\begin{aligned} & \tilde{\mathcal{L}}(\theta^{t+T}, \{\theta_i^{t+T}\}, \{w_i^{t+T}\}, \{\lambda_i^{t+T}\}) - \tilde{\mathcal{L}}(\theta^t, \{\theta_i^t\}, \{w_i^t\}, \{\lambda_i^t\}) \\ & \leq \frac{1}{T} \sum_{i=1}^n \left[-\left(\frac{\rho}{2} - \frac{3L^2}{\rho}\right) \|\theta^{t+T} - \theta^t\|^2 \right. \\ & \quad - \left(\frac{L+\rho}{2} - \frac{12L^2}{\rho}\right) \|\theta_i^{t+T} - \theta_i^t\|^2 \\ & \quad \left. - \left(\frac{L}{2} - \frac{3L^2}{\rho}\right) \|w_i^{t+T} - w_i^t\|^2 \right]. \end{aligned} \quad (13)$$

Proof. The detailed proof can be found in Appendix A. \square

Remark IV.4. Lemma IV.3 shows that if we choose a large enough ρ , the augmented Lagrangian decreases by a sufficient amount after all edge nodes have participated at least once. However, the smoothness parameter is difficult to estimate in practice. We therefore fine-tune ρ from a predefined range of values.

Lemma IV.5 (Lower bound for augmented Lagrangian). *Suppose that the global loss function $\mathcal{L}(\theta, \{w_i\})$ is lower bounded, i.e.,*

$$\underline{\mathcal{L}} := \min_{\theta, \{w_i\}} \mathcal{L}(\theta, \{w_i\}) > -\infty$$

If ρ is chosen large enough that $\rho > 6L$, then the augmented Lagrangian is lower bounded by $\underline{\mathcal{L}}$.

Proof. The detailed proof can be found in Appendix B. \square

Now we combine Lemmas IV.3 and IV.5 to establish the following theorems for the convergence of (12).

Theorem IV.6 (Convergence of the augmented Lagrangian). *Suppose the following are true:*

- After T iterations, all clients have participated in training at least once.
- The global loss function $\mathcal{L}(\theta, \{w_i\})$ is bounded below by a finite quantity $\underline{\mathcal{L}}$.
- The hyperparameter ρ for the augmented Lagrangian is chosen such that $\rho > 6L$.

Then the augmented Lagrangian $\tilde{\mathcal{L}}$ will monotonically decrease and is convergent to a quantity of at least $\underline{\mathcal{L}}$. Further, for all $i = 1, \dots, n$ we have $\lim_{t \rightarrow \infty} \|\theta^{t+T} - \theta_i^{t+T}\| = 0$.

Proof. Lemma IV.3 implies that the augmented Lagrangian decreases by a non-negative amount after every T global iterations. Given Lemma IV.5 and the fact that every client will be updated at least once in the interval $[t, t+T]$, we conclude that the limit $\lim_{t \rightarrow \infty} \tilde{\mathcal{L}}(\theta^{t+T}, \{\theta_i^{t+T}\}, \{w_i^{t+T}\}, \{\lambda_i^{t+T}\})$ exists and is at least $\underline{\mathcal{L}}$.

Now we prove the second statement. From (27) and the fact that $\tilde{\mathcal{L}}$ converges, we conclude that as $t \rightarrow \infty$,

$$\|\theta^{t+T} - \theta^t\| \rightarrow 0, \quad \|\theta_i^{t+T} - \theta_i^t\| \rightarrow 0, \quad \|w_i^{t+T} - w_i^t\| \rightarrow 0.$$

Combining this with (25), we have $\|\lambda_i^{t+1} - \lambda_i^t\| \rightarrow 0$. Based on the definition of λ_i^{t+1} , this implies that $\|\theta_i^{t+1} - \theta^{t+1}\| \rightarrow 0$. \square

Remark IV.7. Theorem IV.6 establishes that the sequence of primal and dual variables updated after each T global iterations of Algorithm 1 converges. Furthermore, we have $\|\theta_i^{t+1} - \theta^{t+1}\| \rightarrow 0$, i.e., the consensus constraint is satisfied.

In the below theorem we present another guarantee that the limit of the sequence $(\theta^t, \{\theta_i^t\}, \{w_i^t\}, \{\lambda_i^t\})$ is the stationary solution for Problem (2).

Theorem IV.8 (Convergence to stationary point). *Suppose the assumptions in Theorem IV.6 hold. Then the limit point $(\theta^*, \{\theta_i^*\}, \{w_i^*\}, \{\lambda_i^*\})$ of the sequence $(\theta^t, \{\theta_i^t\}, \{w_i^t\}, \{\lambda_i^t\})$ is a stationary solution to Problem (2). That is, for all i ,*

$$\begin{aligned} \nabla_{\theta_i} \mathcal{L}_i(\theta^*, w_i^*) + \lambda_i^* &= 0, \\ \nabla_{w_i} \mathcal{L}_i(\theta^*, w_i^*) &= 0, \\ \theta^* &= \theta_i^*. \end{aligned}$$

Proof. See the proof to [46, Theorem 2.4]. \square

Here we make some remarks. First, because Algorithm 1 allows for node sampling on line 5, the proof relies on an assumption that all edge nodes will participate after some fixed number of rounds (in particular, T rounds). Second, since local objectives are non-convex and smooth, the primal variables θ_i and w_i are updated using first-order methods like SGD. Further, the gradient w.r.t. θ_i is found through IFT (lines 12–13), while that w.r.t. w_i only involves a simple backward pass. Finally, the proof aims to show that after every T rounds, we obtain a sufficient decrease in the augmented Lagrangian; coupled with the fact that the augmented Lagrangian is bounded below, the sequence of variables converges to a stationary point of $\tilde{\mathcal{L}}$.

V. EXPERIMENTAL RESULTS

In this section, we present the experimental results and insights into the performance and effectiveness of FeDEQ, demonstrating its advantages compared to existing approaches under various scenarios.

A. Experimental Setup

1) *Datasets and Non-i.i.d. Partition Methods.*: We evaluate FeDEQ on four diverse federated datasets: FEMNIST [47], CIFAR-10 [48], CIFAR-100 [48], and SHAKESPEARE [49]. These datasets cater to various application domains, such as image classification and natural language processing, and are suitable for evaluating FL algorithms in different settings for edge networks. Table I presents the details for the datasets. Here we list some key characteristics of each dataset.

FEMNIST: A variant of the handwritten EMNIST dataset [50] designed specifically for FL. In this work, we use the version obtained from FedJax’s database [51], which simulates real-world non-i.i.d data distributions by writers. The original dataset contains 3,400 writers, providing a total of 780,000 images, with each writer contributing at least one image of each of 62 labels (10 digits and 52 letters). Due to a lack of computing resources, we randomly sample 100 and 200 writers from the original to assign to edge nodes for our experiments.

CIFAR-10: An object recognition dataset [48] including 50,000 training and 10,000 test colored images belonged to 10 classes. The dataset is equally partitioned into 100 nodes in a non-i.i.d. manner, with each node either having data from 2 or 5 distinct classes, depending on the desired scenario. This partitioning simulates real-world FL scenarios facilitating the evaluation of algorithms under heterogeneous data distributions.

CIFAR-100: An object recognition dataset [48] including 50,000 training and 10,000 test colored images belonged to 100 classes. The dataset is divided equally into 100 edge nodes non-i.i.d., with each node having data from either 5 or 20 distinct classes, based on the chosen scenario. This partitioning strategy provides a realistic FL environment, allowing for comprehensive algorithm evaluation with diverse data distributions.

SHAKESPEARE: A federated dataset obtained from FedJax’s database [49] comprising 715 users, representing characters from Shakespeare’s plays, with each example being a series of consecutive lines spoken by a character in a specific play. In this paper, we randomly select 200 edge nodes from the original dataset which each has more than 100 training samples with a sequence length of 16.

2) *Baselines.*: We benchmark FeDEQ against several comparison methods, including locally trained models (Local), the de-facto FedAvg [1], the fine-tuning approach (FedAvg+FT)[20, 21], and four SOTA personalized algorithms including: (1) Ditto [9], an effective full model personalization approach via MTL; (2) FedPer [24] and (3) FedRep [10], emerging partial personalization approaches enabling nodes to collaboratively learn an explicit shared representation and subsequently personalize the local model; and (4) kNN-Per [28], a semi-parametric learning approach that employs kNN as a personalized model on top of pre-trained models. Notably, the latter three are closely

related to ours. We apply settings consistent with FeDEQ for all methods to ensure a fair comparison, and fine-tune their respective hyperparameters to reach their best performance on the settings.

3) *Models and Representations.*: For vision tasks, we construct DEQ-ResNet models inspired by ResNet [52], comprising an equilibrium residual block followed by a 3-layer fully connected (FC) network with the last serving for personalization and using Softplus activations [53], a smooth version of ReLU, to enforce the smoothness assumption in theoretical analysis. We offer two versions of our DEQ-ResNet: "S" (small) and "M" (medium), varying by the size of equilibrium layers. DEQ-ResNet-S is used for FEMNIST and DEQ-ResNet-M for CIFAR-10/CIFAR-100, with FeDEQ. As for other baselines, we employ the architectures of ResNet, using their residual blocks with the same FC network as DEQ-ResNet. Especially, ResNet-20 and ResNet-34 are then employed for experiments on FEMNIST and CIFAR-10/CIFAR-100, correspondingly. For sequence tasks, we design a DEQ-Transformer based on Universal Transformer (UT)[54], consisting of an equilibrium UT block succeeded by a personalized module with one last UT block and one linear layer; while other methods use a UT with 8 layers, 4-head attention (Transformer-8). Specific details regarding the shared parameters and personalized parameters, including the number of model parameters and the model sizes, are presented in Table II and Appendix C.

For training DEQs, we use Anderson Acceleration [41] with warm-start strategy for solving fixed-point system in the forward pass, and Jacobian-free backpropagation [45] for solving the implicit differentiation in the backward pass. It is worth noting that when using non-smooth activations like ReLU, FeDEQ still achieves convergence which reaches similar levels of performance compared to those models using smooth activations.

4) *Training Details.*: Training is proceeded for $T = 150$ communication rounds in the experiments involving FEMNIST, CIFAR-10 and CIFAR-100, whereas for Shakespeare, it is conducted for $T = 400$ rounds. For all methods and experiments, we uniformly sample 10% of nodes without replacement for each round and employ SGD optimizer with a constant learning rate. Unless specified in certain instances, we use 5 local epochs for training shared representation and 3 for personalization for all methods. The final accuracy is determined by averaging local accuracies from all nodes over the last 10 rounds. More details about the training processes are presented in Appendix D.

All experiments are conducted in a coding environment powered by an AMD Ryzen 3970X Processor [55] with 64 cores and 256GB of RAM. Additionally, four NVIDIA GeForce RTX 3090 GPUs [56] are employed to accelerate the training process. For software, we rely on Python3 as our primary language, supplemented by advanced machine learning and optimization frameworks: Jax [57], Haiku [58], Optax [59], Jaxopt [60], and FedJax [51]. Furthermore, our implementation is also inspired by some personalized FL benchmarking works such as Motley [61].

TABLE I: Details on Datasets and Non-i.i.d. Partition Methods

Dataset	Partition Method	Original Nodes	Sample Nodes	Labels/Node	Total Train	Total Test	Mean	Std
FEMNIST	Natural non-i.i.d.	3400	100 200	Various	19,357 39,139	2,237 4,521	194 195	72.9 75.7
CIFAR-10	By-label non-i.i.d.	100	100	2 & 5	50,000	10,000	500	–
CIFAR-100	By-label non-i.i.d.	100	100	5 & 20	50,000	10,000	500	–
SHAKESPEARE	Natural non-i.i.d.	715	200	Various	92,834	11,805	465	506.2

TABLE II: Summary on Shared Representation and Personalization Layers

Datasets	Methods	Shared Representation	Params (M)/ Size (MB)	Personalized Layer	Params (M)/ Size (MB)
FEMNIST	Baselines	ResNet-20 (19 Conv + 2 FC)	2.97 / 11.87	1 FC	0.008 / 0.03
	FeDEQ	DEQ-ResNet-S (3 Conv + 2 FC)	0.98 / 3.94	1 FC	0.008 / 0.03
CIFAR-10	Baselines	Resnet-34 (33 Conv + 2 FC)	7.78 / 31.11	1 FC	0.001/0.01
	FeDEQ	DEQ-Resnet-M (3 Conv + 2 FC)	2.73 / 10.90	1 FC	0.001/0.01
CIFAR-100	Baselines	Resnet-34 (33 Conv + 2 FC)	10.88 / 43.51	1 FC	0.01/0.05
	FeDEQ	DEQ-Resnet-M (3 Conv + 2 FC)	2.73 / 10.90	1 FC	0.01/0.05
ShakeSpear	Baselines	Transformer-8 (8 UT, 4 H)	0.35 / 1.43	1 UT + 1 FC	0.06/0.22
	FeDEQ	DEQ-Transformer (4 UT, 4 H)	0.21 / 0.83	1 UT + 1 FC	0.06/0.22

Acronym: Conv – Convolutional layer; FC – Fully Connected layer; UT – Universal Transformer layer; H – Head-attention; Params – The number of model parameters; M – Millions; Size – The size of model; MB – Megabytes

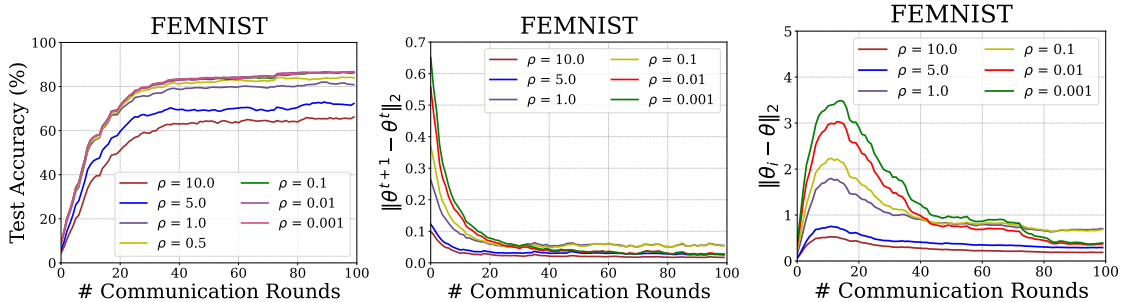


Fig. 5: Effects of ρ on the convergence of the shared representation θ

B. Results and Evaluation

1) *Effects of ρ on the performance of FeDEQ.*: The penalty parameter ρ in FeDEQ is a tuning parameter that controls the trade-off between the dual constraint satisfaction (i.e., how closely the local representation matches the shared representation) and the minimization of the objective function. Therefore, the selection of ρ is crucial for the performance of FeDEQ and it can vary significantly based on the specific optimization problem. To investigate the impact of ρ FeDEQ’s performance and convergence, we vary ρ values within $\{0.001, 0.01, 0.1, 1.0, 5.0, 10.0\}$ on the FEMNIST dataset.

The results in Fig. 5 show that FeDEQ achieves convergence with any ρ within the range; however, if ρ is too small, the constraint $\theta_i = \theta$ is weakly enforced, meaning that the local variables have more freedom to minimize their local objective function, which might cause the consensus variable to deviate from the optimum. This might increase the number of iterations needed for convergence (e.g., $\rho = 0.001$) or may even prevent convergence in certain cases. On the other hand, it can provide a better local performance as each subproblem can be more optimized according to its local data. Conversely,

if ρ is too large, the algorithm will strongly enforce the consensus constraint, which can lead to a swift alignment of the local variables to the consensus variable (e.g., $\rho = 5.0$ or $\rho = 10.0$). However, this might cause suboptimal solutions because the strong enforcement of the consensus might prevent local variables from reaching their local optima. In other words, it imposes high “pressure” to force local solutions to agree, potentially at the expense of solution quality.

Through empirical evaluation, we found that $\rho = 0.01$ provides the best balance for our datasets. In practice, selecting a suitable ρ often involves trial and error or a validation process. It is also possible to use an adaptive strategy, where ρ is updated during the optimization process.

2) *The convergence of FeDEQ.*: To empirically assess the convergence of FeDEQ across all the datasets, we provide both the test accuracy and the training loss (using the function \mathcal{L}) over global communication rounds in Fig. 6,7. Those figures reveal a consistent trend: across all datasets, FeDEQ’s loss decreased and stabilized within a dataset-specific range of communication rounds, signaling a stable and reliable convergence trajectory. Specially, for the FEMNIST dataset,

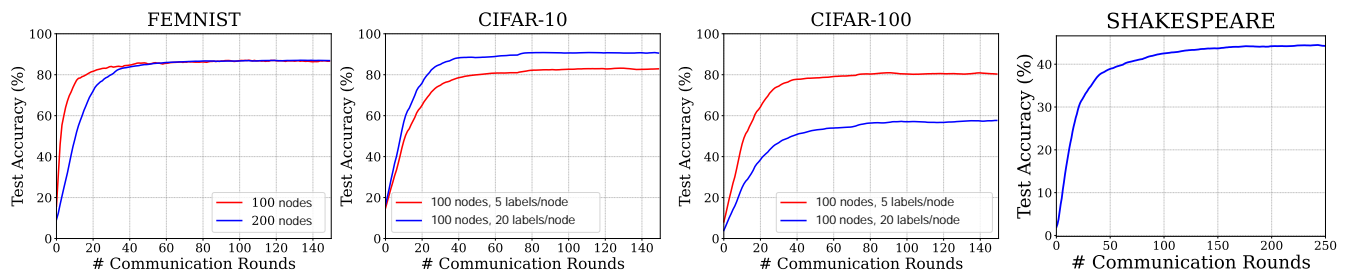


Fig. 6: Test accuracy of FeDEQ across the datasets.

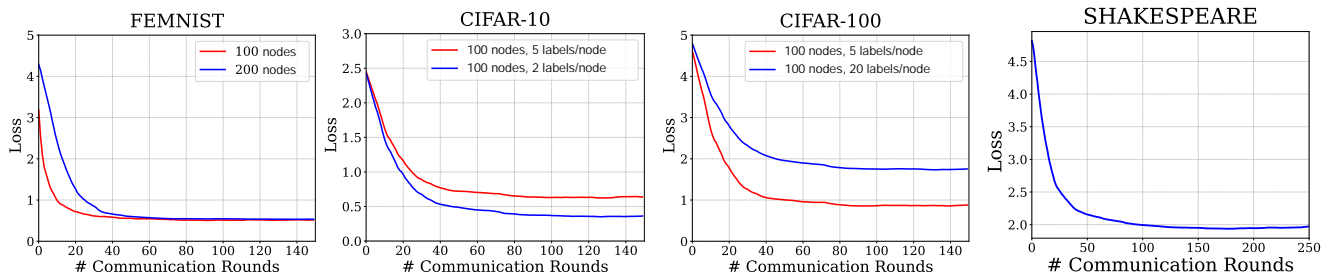


Fig. 7: Average loss of FeDEQ across the datasets.

convergence was observed by the 50th communication round, achieving a test accuracy of approximately 87%. In the case of CIFAR-10, despite its inherent challenges, FeDEQ exhibited convergence by the 80th round, with test accuracies reaching up to 90%. The CIFAR-100 dataset, with its augmented label complexity, presented a more intricate challenge. Nevertheless, convergence was achieved around the same 80th round, with test accuracies ranging between 58% and 80%, contingent on the label distribution. The Shakespeare dataset, distinct in its data distribution, witnessed convergence by the 120th round and realized an accuracy of approximately 48%. These empirical findings not only attest to the adaptability and resilience of FeDEQ but also position it as a promising solution for a myriad of federated learning scenarios.

3) *Model Size and Communication Efficiency.*: In edge networks, the implementation of FL often confronts formidable communication challenges. Such challenges arise from the recurring necessity to update and transmit large and deep model parameters during the training process. Here, we highlight the prowess of FeDEQ in achieving efficient communication, even with compact model size, without compromising on performance excellence. Specially, we examine the efficacy of FeDEQ with DEQs, in comparison to FedRep with explicit models. For our experiments with FeDEQ, we utilize DEQ-ResNet-S for FEMNIST, DEQ-ResNet-M for both CIFAR-10 and CIFAR-100 and DEQ-Transformer for the Shakespeare dataset. In contrast, for FedRep, we delve into a range of models from more compact architectures (e.g., ResNet-14, Transformer-4) to their intricate counterparts (e.g., ResNet-34, Transformer-12), across various datasets.

The results shown in Fig. 8 reveal that FeDEQ consistently maintains a smaller model size for all datasets while achieving competitive accuracy levels. In FEMNIST, FeDEQ with DEQ-ResNet-S outperforms FedRep using the ResNet-14 model, which is 1.5 times larger in size. Remarkably, even with a model

size that is 2 – 4 times smaller, FeDEQ achieves performance metrics comparable to deeper architectures, such as ResNet-20 and ResNet-34. This trend of maintaining compactness without compromising accuracy is consistently observed in CIFAR-10 and CIFAR-100, where FeDEQ either matches or slightly exceeds the performance of other benchmarked models. Furthermore, in the Shakespeare dataset, FeDEQ’s implementation with DEQ-Transformer consistently presents a model that is up to 3 times more compact than standard Transformers, yet the accuracy remains competitive.

These findings underscore FeDEQ’s potential as a robust solution for edge environments that prioritize both model efficiency and performance. A smaller model size implies more efficient update exchanges in FL scenarios, an essential aspect in edge environments characterized by limited bandwidth and computational resources. The compact nature of FeDEQ ensures that edge devices engage in communication processes that are both resource-efficient and rapid, thereby facilitating expedited decision-making.

4) *Performance of Personalized Models.*: To investigate how FeDEQ addresses the data heterogeneity issue through personalization, we evaluate the performance of FeDEQ and various baselines on the local test datasets of edge nodes (unseen during training) across a range of tasks, as detailed in Table III. As anticipated, FeDEQ consistently outperforms non-personalized methods (Local, FedAvg, and FedAvg+FT), which generally exhibit lower performance compared to personalized approaches in the context of data heterogeneity. Taking the FEMNIST dataset as an example, while the best non-personalized algorithm, FedAvg+FT, achieves accuracies of 84.98% for 100 nodes and 85.40% for 200 nodes, FeDEQ impressively scores 87.13% and 87.46% respectively, demonstrating a clear advantage in the realm of approximately 18%.

When pitted against personalized FL baselines, FeDEQ showcases competitive performance with Ditto and faintly

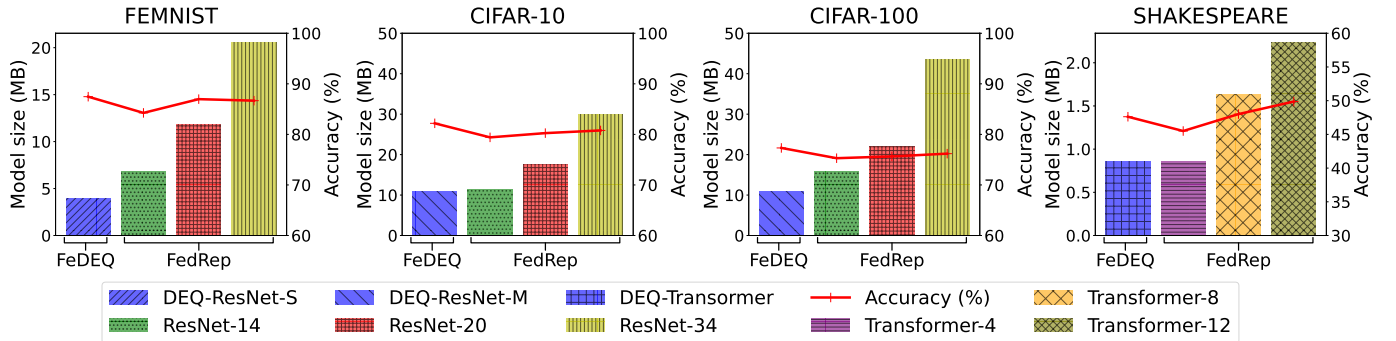


Fig. 8: Comparison the model size and accuracy of FeDEQ and FedRep across the datasets.

TABLE III: Test accuracy of different algorithms across edge nodes

Datasets (c, p) [†]	FEMNIST		CIFAR-10		CIFAR-100		Shakespeare
	(100, -)	(200, -)	(100, 2)	(100, 5)	(100, 5)	(100, 20)	(200, -)
Local	68.80	68.77	83.85	65.78	66.67	34.93	28.70
FedAvg	83.50	82.12	38.91	63.78	33.05	33.06	48.07
FedAvg + FT	84.98	85.40	88.75	79.88	77.14	55.71	46.60
Ditto	<u>87.93</u>	<u>88.43</u>	90.27	82.18	80.37	57.18	47.56
FedPer	85.10	85.42	87.89	80.38	78.88	55.07	44.66
FedRep	85.29	86.18	87.81	80.25	79.53	56.30	48.01
kNN-Per	84.94	85.36	87.43	80.18	76.19	56.27	<u>48.77</u>
FeDEQ (Ours)	87.13	87.46	90.54	82.84	80.42	57.49	47.62

[†] (c, p) corresponding to c nodes and p classes per node). For FEMNIST and Shakespeare, p might be various denoted by "-".

surpasses FedPer, FedRep, and kNN-Per. On FEMNIST dataset, FeDEQ achieves accuracies faintly less than Ditto but outshines the other methods. In the CIFAR-10 dataset with various degrees of heterogeneity, FeDEQ achieves top accuracies of 90.54% and 82.84% respectively. These results marginally surpass the performance of other personalized algorithms like Ditto, which scores 90.27% and 82.18% under the same conditions. Similarly, for the CIFAR-100 dataset, FeDEQ’s performance peaks at 80.42% and 57.49% for configurations (100, 5) and (100, 20), respectively, again nudging past the closest competitor, Ditto, which posts figures of 80.37% and 57.18%. Furthermore, in the next-character prediction task, while kNN-Per achieves the highest accuracy, FeDEQ closely follows with a small gap, exhibiting competitiveness. Consequently, FeDEQ consistently delivers comparable or superior performance with SOTA algorithms across all datasets, while offering substantial efficiency in terms of communication with up to 4 times smaller in the size of representation.

5) *Generalization to new edge nodes.*: We demonstrate the benefits of the shared representation in generalizing to new, unseen edge nodes. To achieve this, we split the edge nodes into two groups: 90% training nodes, and 10% new, unseen nodes. Initially, we train the shared representation for FeDEQ, FedPer FedRep, and kNN-Per using the designated training group, then use it to refine the personalization layers for new nodes using their training data, which has not been incorporated during the representation training process. For FedAvg and Ditto, a full

model will be trained and adapted to new participants. Table IV presents the performance of these new edge nodes.

Notably, kNN-Per underperforms FedPer and FedRep in vision tasks as its shared representation is trained from scratch rather than using pre-trained models as in the original proposal, but excels all in the sequence task. Despite Ditto showcases effective personalization on training nodes, it falls short when dealing with new nodes. Meanwhile, FeDEQ demonstrates remarkable competitiveness, consistently surpassing the other algorithms on FEMNIST, CIFAR-10, CIFAR-100 while keeping acceptable performance on Shakespeare. This implies that the shared representation facilitated by FeDEQ possesses the capacity for effective adaptation to newly joined nodes, even with a significantly reduced size.

6) *Effects of Shared Representation on Personalization*: Our investigation turns towards assessing the robustness and adaptability of the shared representation learned by FeDEQ, FedPer, and FedRep, particularly on the FEMNIST and CIFAR-10 datasets. For a comprehensive assessment, two tailored scenarios have been meticulously designed. In the first scenario, we vary the local epochs for updating personalized parameters while keeping a constant number of epochs for training the shared representation. As depicted in Fig. 9a,9c, in FEMNIST, all methods only require a few personalized epochs to reach peak performance due to the simplicity of the dataset; however, overfitting becomes a concern shortly thereafter. Meanwhile, in CIFAR-10, FeDEQ achieves desirable results with fewer

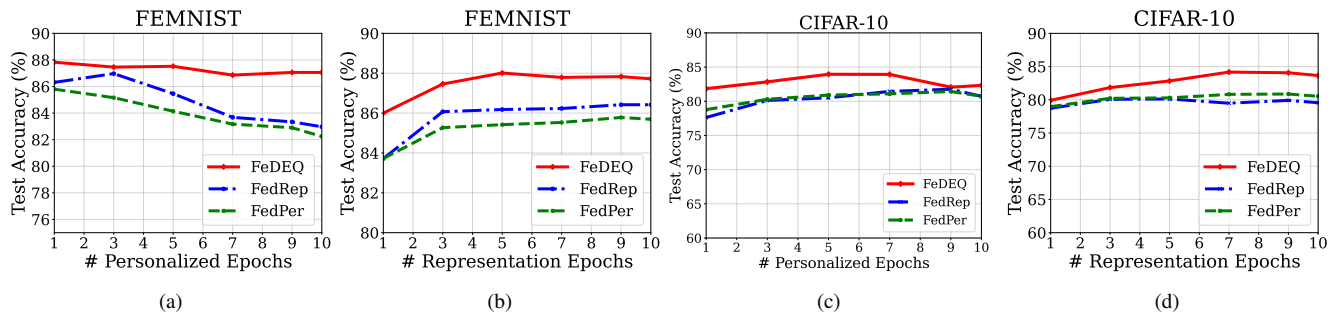


Fig. 9: Effects of Shared Representation on Personalization in FEMNIST (a, b) and CIFAR-10 (c, d)

TABLE IV: Test accuracy across unseen edge nodes (test accuracy of training nodes between parentheses)

Datasets (c, u, p) [†]	FEMNIST	CIFAR-10	CIFAR-100	Shakespeare
Algorithms	(180, 20, -)	(90, 10, 5)	(90, 10, 20)	(180, 20, -)
FedAvg	80.04 (82.30)	50.20 (57.76)	28.40 (28.90)	46.92 (47.68)
Ditto	81.65 (88.70)	50.90 (82.34)	29.60 (55.86)	47.20 (47.24)
FedPer	83.47 (85.20)	78.20 (79.63)	59.20 (52.82)	45.47 (44.53)
FedRep	84.68 (86.12)	78.90 (79.11)	57.40 (52.97)	47.89 (48.00)
kNN-Per	84.48 (85.40)	75.70 (80.72)	50.70 (53.73)	<u>48.26</u> (48.59)
FeDEQ (Ours)	85.69 (87.00)	79.20 (83.18)	60.10 (54.22)	47.25 (47.46)

[†] (c, u, p) corresponding to c training nodes, u unseen nodes and p classes per node. For FEMNIST and Shakspeare, p might be various denoted by ”-”.

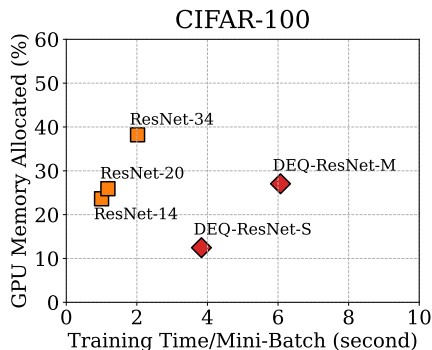


Fig. 10: Memory usage vs. training time of DEQ-ResNets and ResNets.

personalized updates than the others.

In the second scenario, the emphasis is shifted towards the epochs for training the shared representation while the epochs for personalized parameter updates are kept constant. We observe that a satisfactory shared representation could be achieved within a few epochs across all methods on both datasets, but FeDEQ potentially needs fewer to attain a good one, as shown in Fig. 9b,9d. These results imply that FeDEQ can learn representations more effectively than its explicit counterparts. Furthermore, FeDEQ’s performance consistently surpasses the others in both scenarios, highlighting its ability to maintain stable performance on personalization.

7) *Memory and Time Complexity.*: As FL to be deployed the network edge, efficient memory management has become a non-negotiable criterion, especially in scenarios with resource constraints. DEQs which are recognized for their consistent memory footprints during training phases, emerge as a promis-

ing solution in this context [30]. To demonstrate that, we measure the average GPU memory consumption during training FedAvg with DEQ-ResNets on edge nodes using the CIFAR-100 dataset, in comparison to FedAvg with explicit ResNet models. Fig. 10 reveals that DEQ-ResNet-S has the lowest memory footprint due to its smaller size. DEQ-ResNet-M’s memory usage is roughly on par with ResNet-14 and ResNet-20, but nearly 1.5 times lower than ResNet-34 for training each mini-batch. This can be attributed to DEQs’ reliance on implicit differentiation, which eliminates the need to store intermediate values of all layers for backpropagation.

Limitations. While the memory benefits of FeDEQ are significant, the biggest drawback of FeDEQ lies in the training time, which is approximately 2 – 3 times slower than explicit models (Fig. 10) due to the iterative nature of solving DEQ’s forward and backward pass. To mitigate this, we can explore acceleration methods for solving fixed-point iterations or implicit differentiation.

VI. CONCLUSION

The challenges of data heterogeneity, communication bottlenecks, and memory constraints are well-known in FL at the network edge. While existing works have extensively addressed each problem—such as using model personalization for data heterogeneity or model compression to reduce communication cost—a comprehensive solution to address these challenges is underexplored. In this paper, we introduce FeDEQ, a novel approach for FL that aims to tackle these challenges concurrently. The design of FeDEQ benefits from the compactness and representation power of deep equilibrium models and the

personalization capabilities of local fine-tuning. We formulate an ADMM consensus optimization scheme that allows edge nodes to learn a shared representation and then adapt to their personalized parameters. Extensive experiments on various benchmarks showcase FeDEQ’s ability to achieve comparable performance to state-of-the-art methods with explicit models of up to four times larger in size, highlighting FeDEQ’s lower memory footprint during training and hence a direct benefit to communication in FL for edge environments.

REFERENCES

- [1] B. McMahan, E. Moore, D. Ramage, S. Hampson, and B. A. y. Arcas, “Communication-Efficient Learning of Deep Networks from Decentralized Data,” in *Proceedings of the 20th International Conference on Artificial Intelligence and Statistics*, ser. Proceedings of Machine Learning Research, A. Singh and J. Zhu, Eds., vol. 54. PMLR, 20–22 Apr 2017, pp. 1273–1282.
- [2] F. Sattler, S. Wiedemann, K.-R. Müller, and W. Samek, “Robust and communication-efficient federated learning from non-i.i.d. data,” *IEEE Transactions on Neural Networks and Learning Systems*, vol. 31, no. 9, pp. 3400–3413, 2020.
- [3] A. Reisizadeh, A. Mokhtari, H. Hassani, A. Jadbabaie, and R. Pedarsani, “Fedpaq: A communication-efficient federated learning method with periodic averaging and quantization,” in *Proceedings of the Twenty Third International Conference on Artificial Intelligence and Statistics*, ser. Proceedings of Machine Learning Research, S. Chiappa and R. Calandra, Eds., vol. 108. PMLR, 26–28 Aug 2020, pp. 2021–2031.
- [4] Y. Wang, L. Lin, and J. Chen, “Communication-efficient adaptive federated learning,” in *Proceedings of the 39th International Conference on Machine Learning*, ser. Proceedings of Machine Learning Research, K. Chaudhuri, S. Jegelka, L. Song, C. Szepesvari, G. Niu, and S. Sabato, Eds., vol. 162. PMLR, 17–23 Jul 2022, pp. 22 802–22 838.
- [5] A. Fallah, A. Mokhtari, and A. Ozdaglar, “Personalized federated learning with theoretical guarantees: A model-agnostic meta-learning approach,” in *Proceedings of the 34th International Conference on Neural Information Processing Systems*, ser. NIPS’20. Red Hook, NY, USA: Curran Associates Inc., 2020.
- [6] C. T. Dinh, N. H. Tran, and T. D. Nguyen, “Personalized federated learning with moreau envelopes,” in *Proceedings of the 34th International Conference on Neural Information Processing Systems*, ser. NIPS’20. Red Hook, NY, USA: Curran Associates Inc., 2020.
- [7] V. Smith, C.-K. Chiang, M. Sanjabi, and A. Talwalkar, “Federated Multi-Task Learning,” *arXiv:1705.10467 [cs, stat]*, Feb. 2018, arXiv: 1705.10467.
- [8] O. Marfoq, G. Neglia, A. Bellet, L. Kameni, and R. Vidal, “Federated multi-task learning under a mixture of distributions,” 2021.
- [9] T. Li, S. Hu, A. Beirami, and V. Smith, “Ditto: Fair and robust federated learning through personalization,” in *International Conference on Machine Learning*, 2020.
- [10] L. Collins, H. Hassani, A. Mokhtari, and S. Shakkottai, “Exploiting shared representations for personalized federated learning,” in *Proceedings of the 38th International Conference on Machine Learning*, ser. Proceedings of Machine Learning Research, M. Meila and T. Zhang, Eds., vol. 139. PMLR, 18–24 Jul 2021, pp. 2089–2099.
- [11] K. Pillutla, K. Malik, A.-R. Mohamed, M. Rabbat, M. Sanjabi, and L. Xiao, “Federated learning with partial model personalization,” in *Proceedings of the 39th International Conference on Machine Learning*, ser. Proceedings of Machine Learning Research, K. Chaudhuri, S. Jegelka, L. Song, C. Szepesvari, G. Niu, and S. Sabato, Eds., vol. 162. PMLR, 17–23 Jul 2022, pp. 17 716–17 758.
- [12] J. Konečný, H. B. McMahan, F. X. Yu, P. Richtárik, A. T. Suresh, and D. Bacon, “Federated Learning: Strategies for Improving Communication Efficiency,” *arXiv:1610.05492 [cs]*, Oct. 2017, arXiv: 1610.05492.
- [13] A. T. Suresh, F. X. Yu, S. Kumar, and H. B. McMahan, “Distributed Mean Estimation with Limited Communication,” *arXiv:1611.00429 [cs]*, Sep. 2017, arXiv: 1611.00429.
- [14] A. Reisizadeh, A. Mokhtari, H. Hassani, A. Jadbabaie, and R. Pedarsani, “Fedpaq: A communication-efficient federated learning method with periodic averaging and quantization,” in *Proceedings of the Twenty Third International Conference on Artificial Intelligence and Statistics*, ser. Proceedings of Machine Learning Research, S. Chiappa and R. Calandra, Eds., vol. 108. PMLR, 26–28 Aug 2020, pp. 2021–2031.
- [15] Y. Zhao, M. Li, L. Lai, N. Suda, D. Civin, and V. Chandra, “Federated Learning with Non-IID Data,” *arXiv:1806.00582 [cs, stat]*, Jun. 2018, arXiv: 1806.00582.
- [16] X. Li, K. Huang, W. Yang, S. Wang, and Z. Zhang, “On the Convergence of FedAvg on Non-IID Data,” *arXiv:1907.02189 [cs, math, stat]*, Jun. 2020, arXiv: 1907.02189.
- [17] T. Yoon, S. Shin, S. J. Hwang, and E. Yang, “Fedmix: Approximation of mixup under mean augmented federated learning,” in *International Conference on Learning Representations*, 2021.
- [18] S. P. Karimireddy, S. Kale, M. Mohri, S. Reddi, S. Stich, and A. T. Suresh, “SCAFFOLD: Stochastic controlled averaging for federated learning,” in *Proceedings of the 37th International Conference on Machine Learning*, ser. Proceedings of Machine Learning Research, H. D. III and A. Singh, Eds., vol. 119. PMLR, 13–18 Jul 2020, pp. 5132–5143.
- [19] A. Z. Tan, H. Yu, L. zhen Cui, and Q. Yang, “Towards personalized federated learning,” *IEEE Transactions on Neural Networks and Learning Systems*, vol. PP, 2021.
- [20] Y. Jiang, J. Konečný, K. Rush, and S. Kannan, “Improving federated learning personalization via model agnostic meta learning,” *ArXiv*, vol. abs/1909.12488, 2019.
- [21] L. Collins, H. Hassani, A. Mokhtari, and S. Shakkottai, “Fedavg with fine tuning: Local updates lead to representation learning,” 2022.
- [22] F. Hanzely and P. Richtárik, “Federated learning of

- a mixture of global and local models,” *ArXiv*, vol. abs/2002.05516, 2020.
- [23] Y. Deng, M. M. Kamani, and M. Mahdavi, “Adaptive personalized federated learning,” *CoRR*, vol. abs/2003.13461, 2020.
- [24] M. G. Arivazhagan, V. Aggarwal, A. K. Singh, and S. Choudhary, “Federated learning with personalization layers,” *CoRR*, vol. abs/1912.00818, 2019.
- [25] F. Hanzely, B. Zhao, and M. Kolar, “Personalized federated learning: A unified framework and universal optimization techniques,” *CoRR*, vol. abs/2102.09743, 2021.
- [26] K. Singhal, H. Sidahmed, Z. Garrett, S. Wu, J. K. Rush, and S. Prakash, “Federated reconstruction: Partially local federated learning,” in *Advances in Neural Information Processing Systems*, A. Beygelzimer, Y. Dauphin, P. Liang, and J. W. Vaughan, Eds., 2021.
- [27] S. Lin, Y. Han, X. Li, and Z. Zhang, “Personalized federated learning towards communication efficiency, robustness and fairness,” in *Advances in Neural Information Processing Systems*, A. H. Oh, A. Agarwal, D. Belgrave, and K. Cho, Eds., 2022.
- [28] O. Marfoq, G. Neglia, R. Vidal, and L. Kameni, “Personalized federated learning through local memorization,” in *Proceedings of the 39th International Conference on Machine Learning*, ser. Proceedings of Machine Learning Research, K. Chaudhuri, S. Jegelka, L. Song, C. Szepesvari, G. Niu, and S. Sabato, Eds., vol. 162. PMLR, 17–23 Jul 2022, pp. 15 070–15 092.
- [29] I. Achituve, A. Shamsian, A. Navon, G. Chechik, and E. Fetaya, “Personalized federated learning with gaussian processes,” in *Advances in Neural Information Processing Systems*, A. Beygelzimer, Y. Dauphin, P. Liang, and J. W. Vaughan, Eds., 2021.
- [30] S. Bai, J. Z. Kolter, and V. Koltun, “Deep equilibrium models,” in *Advances in Neural Information Processing Systems*, H. Wallach, H. Larochelle, A. Beygelzimer, F. d’Alché-Buc, E. Fox, and R. Garnett, Eds., vol. 32. Curran Associates, Inc., 2019.
- [31] L. El Ghaoui, F. Gu, B. Travacca, A. Askari, and A. Tsai, “Implicit deep learning,” *SIAM Journal on Mathematics of Data Science*, vol. 3, no. 3, pp. 930–958, 2021.
- [32] K. Kawaguchi, “On the theory of implicit deep learning: Global convergence with implicit layers,” in *International Conference on Learning Representations*, 2021.
- [33] S. Bai, V. Koltun, and J. Z. Kolter, “Multiscale deep equilibrium models,” in *Advances in Neural Information Processing Systems*, H. Larochelle, M. Ranzato, R. Hassel, M. Balcan, and H. Lin, Eds., vol. 33. Curran Associates, Inc., 2020, pp. 5238–5250.
- [34] S. Boyd, N. Parikh, E. Chu, B. Peleato, and J. Eckstein, “Distributed optimization and statistical learning via the alternating direction method of multipliers,” *Found. Trends Mach. Learn.*, vol. 3, no. 1, p. 1–122, jan 2011.
- [35] X. Zhang, M. M. Khalili, and M. Liu, “Improving the privacy and accuracy of ADMM-based distributed algorithms,” in *Proceedings of the 35th International Conference on Machine Learning*, ser. Proceedings of Machine Learning Research, J. Dy and A. Krause, Eds., vol. 80. PMLR, 10–15 Jul 2018, pp. 5796–5805.
- [36] A. Elgabli, J. Park, S. Ahmed, and M. Bennis, “L-fgadm: Layer-wise federated group adm for communication efficient decentralized deep learning,” *2020 IEEE Wireless Communications and Networking Conference (WCNC)*, pp. 1–6, 2019.
- [37] S. Zhou and G. Y. Li, “Communication-efficient adm-based federated learning,” *CoRR*, vol. abs/2110.15318, 2021.
- [38] S. Yue, J. Ren, J. Xin, S. Lin, and J. Zhang, “Inexact-admm based federated meta-learning for fast and continual edge learning,” in *Proceedings of the Twenty-Second International Symposium on Theory, Algorithmic Foundations, and Protocol Design for Mobile Networks and Mobile Computing*, ser. MobiHoc ’21. New York, NY, USA: Association for Computing Machinery, 2021, p. 91–100.
- [39] K. Ciesielski, “On Stefan Banach and some of his results,” *Banach Journal of Mathematical Analysis*, vol. 1, no. 1, pp. 1 – 10, 2007.
- [40] C. G. Broyden, “A class of methods for solving nonlinear simultaneous equations,” *Mathematics of Computation*, vol. 19, pp. 577–593, 1965.
- [41] H. F. Walker and P. Ni, “Anderson acceleration for fixed-point iterations,” *SIAM Journal on Numerical Analysis*, vol. 49, no. 4, pp. 1715–1735, 2011.
- [42] S. Bai, V. Koltun, and J. Z. Kolter, “Neural deep equilibrium solvers,” in *International Conference on Learning Representations*, 2022.
- [43] M. Z. K. Johnson, David Duvenaud, “Chapter 4: Deep Equilibrium Models.”
- [44] M. R. Hestenes and E. Stiefel, “Methods of conjugate gradients for solving linear systems,” *Journal of research of the National Bureau of Standards*, vol. 49, pp. 409–435, 1952.
- [45] S. W. Fung, H. Heaton, Q. Li, D. Mckenzie, S. J. Osher, and W. Yin, “Jfb: Jacobian-free backpropagation for implicit networks,” in *AAAI Conference on Artificial Intelligence*, 2021.
- [46] M. Hong, Z.-Q. Luo, and M. Razaviyayn, “Convergence analysis of alternating direction method of multipliers for a family of nonconvex problems,” *SIAM Journal on Optimization*, vol. 26, no. 1, pp. 337–364, 2016.
- [47] S. Caldas, S. M. K. Duddu, P. Wu, T. Li, J. Konečný, H. B. McMahan, V. Smith, and A. Talwalkar, “Leaf: A benchmark for federated settings,” in *Workshop on Federated Learning for Data Privacy and Confidentiality*, 2019.
- [48] A. Krizhevsky, “Learning Multiple Layers of Features from Tiny Images,” p. 60, 2009.
- [49] B. McMahan, E. Moore, D. Ramage, S. Hampson, and B. A. y Arcas, “Communication-efficient learning of deep networks from decentralized data,” in *Artificial Intelligence and Statistics*. PMLR, 2017, pp. 1273–1282.
- [50] G. Cohen, S. Afshar, J. Tapson, and A. Van Schaik, “Emnist: Extending mnist to handwritten letters,” in *2017 International Joint Conference on Neural Networks (IJCNN)*. IEEE, 2017, pp. 2921–2926.

- [51] G. Wang, H. Yu, S. Wu, W. Dai, J. Feng, S. Li, H. Yu, T. Li, and J. Konečný, “Fedjax: Federated learning simulation with jax,” 2021.
- [52] K. He, X. Zhang, S. Ren, and J. Sun, “Deep residual learning for image recognition,” *CoRR*, vol. abs/1512.03385, 2015.
- [53] C. Dugas, Y. Bengio, F. Bélisle, C. Nadeau, and R. Garcia, “Incorporating second-order functional knowledge for better option pricing,” in *Advances in Neural Information Processing Systems*, T. Leen, T. Dietterich, and V. Tresp, Eds., vol. 13. MIT Press, 2000.
- [54] M. Dehghani, S. Gouws, O. Vinyals, J. Uszkoreit, and L. Kaiser, “Universal transformers,” in *International Conference on Learning Representations*, 2019.
- [55] “AMD Ryzen™ Threadripper™ 3970X Drivers & Support | AMD,” May 2022.
- [56] “Geforce rtx 3090 family - 3090 & 3090 Ti Graphics Cards.”
- [57] J. Bradbury, R. Frostig, P. Hawkins *et al.*, “JAX: composable transformations of Python+NumPy programs,” 2018.
- [58] T. Hennigan, T. Cai, T. Norman, and I. Babuschkin, “Haiku: Sonnet for JAX,” 2020.
- [59] I. Babuschkin, K. Baumli, A. Bell *et al.*, “The DeepMind JAX Ecosystem,” 2020.
- [60] M. Blondel, Q. Berthet, M. Cuturi, R. Frostig, S. Hoyer, F. Llinares-Lopez, F. Pedregosa, and J.-P. Vert, “Efficient and modular implicit differentiation,” in *Advances in Neural Information Processing Systems*, S. Koyejo, S. Mohamed, A. Agarwal, D. Belgrave, K. Cho, and A. Oh, Eds., vol. 35. Curran Associates, Inc., 2022, pp. 5230–5242.
- [61] S. Wu, T. Li, Z. Charles, Y. Xiao, Z. Liu, Z. Xu, and V. Smith, “Motley: Benchmarking heterogeneity and personalization in federated learning,” 2022.

APPENDIX

First, we restate the original optimization problem. Let the local loss function on each edge node be $\mathcal{L}_i(\theta, w_i) := \frac{1}{n_i} \sum_{j=1}^{n_i} \ell(f_{\theta, w_i}(x_{ij}), y_{ij})$, where θ is the parameters to be shared in the implicit module and w_i is the local parameters w.r.t. to the personalized module. The objective is to minimize the the global loss function as follows

$$\min_{\theta, \{w_i\}} \left\{ \mathcal{L}(\theta, \{w_i\}) := \sum_{i=1}^n \mathcal{L}_i(\theta, w_i) \right\}.$$

We reframe this problem as an equivalent consensus optimization scheme:

$$\min_{\{\theta_i, \{w_i\}, \theta} \sum_{i=1}^n \mathcal{L}_i(\theta_i, w_i) \quad \text{s.t.} \quad \theta_i = \theta, \quad \forall i, \quad (14)$$

where θ_i and w_i are the local parameters on edge node i . The enforcement of the constraints $\theta_i = \theta, \forall i$ is to encourage the learning of a common representation module θ that benefits from all edge nodes' data. On the other hand, w_i is not shared as it is used specifically for personalization on edge node i .

Recognizing that (14) is a consensus optimization problem, we employ alternating direction method method of multipliers (ADMM) to solve it. This algorithm is based on alternating updates of primal and dual variables to achieve two goals: θ_i across edge nodes become closer and the objective function decreases. An introduction to ADMM can be found in [34]. Applying this to our problem, we first construct the *augmented Lagrangian* for each edge node i as

$$\tilde{\mathcal{L}}_i(\theta, \theta_i, w_i, \lambda_i) := \mathcal{L}_i(\theta_i, w_i) + \langle \lambda_i, \theta_i - \theta \rangle + \frac{\rho}{2} \|\theta_i - \theta\|^2, \quad (15)$$

where λ_i is the dual variable associated with the constraint $\theta_i = \theta$, and $\rho > 0$ is a hyperparameter. (We will discuss the effect of ρ in the following discussion.) All inner products and norms are Euclidean. Note that we do not have a dual variable for w_i because it is not shared. Given this, we define the global augmented Lagrangian as

$$\tilde{\mathcal{L}}(\theta, \{\theta_i\}, \{w_i\}, \{\lambda_i\}) := \sum_{i=1}^n \tilde{\mathcal{L}}_i(\theta, \theta_i, w_i, \lambda_i). \quad (16)$$

Algorithm 1 in the main text describes the ADMM procedure. First, all variables $(\theta^0, \theta_i^0, w_i^0, \lambda_i^0)$ are initialized randomly. In each *global iteration* t (line 3), we have the current variables $\theta^t, \theta_i^t, w_i^t, \lambda_i^t$ and will update them as follows:

- The server aggregates θ_i^t from a selected subset of edge nodes S_t : $\theta^{t+1} = \frac{1}{|S_t|} \sum_{i \in S_t} \theta_i^t$ (line 4). Then the server samples a new edge node subset S_{t+1} and sends the new θ^{t+1} to them (lines 5–7).
- Each chosen node in S_{t+1} aims to minimize its local augmented Lagrangian $\tilde{\mathcal{L}}_i(\theta^{t+1}, \theta_i, w_i, \lambda_i^t)$ w.r.t. its parameters θ_i and w_i (lines 8–9). This gives the new variables θ_i^{t+1} and w_i^{t+1} .
- Finally, each chosen node updates its dual variable λ_i using the ascent step: $\lambda_i^{t+1} = \lambda_i^t + \rho(\theta_i^{t+1} - \lambda_i^t)$ (line 10).

Here, we proceed to show that the sequence of variables $(\theta^t, \{\theta_i^t\}, \{w_i^t\}, \{\lambda_i^t\})$ converges to the set of stationary points

of the augmented Lagrangian, concluding our proof. In particular, we aim to show that the augmented Lagrangian sufficiently decreases over time (Appendix A). In addition, $\tilde{\mathcal{L}}$ is lower bounded by the minimum of the global loss function \mathcal{L} (Appendix B).

A. Proof of Lemma IV.3

Proof. First, the change in the augmented Lagrangian after one global round can be decomposed as follows

$$\begin{aligned} & \tilde{\mathcal{L}}(\theta^{t+1}, \{\theta_i^{t+1}\}, \{w_i^{t+1}\}, \{\lambda_i^{t+1}\}) - \tilde{\mathcal{L}}(\theta^t, \{\theta_i^t\}, \{w_i^t\}, \{\lambda_i^t\}) \\ &= \left(\tilde{\mathcal{L}}(\theta^{t+1}, \{\theta_i^t\}, \{w_i^t\}, \{\lambda_i^t\}) - \tilde{\mathcal{L}}(\theta^t, \{\theta_i^t\}, \{w_i^t\}, \{\lambda_i^t\}) \right) \\ & \quad + \left(\tilde{\mathcal{L}}(\theta^{t+1}, \{\theta_i^{t+1}\}, \{w_i^{t+1}\}, \{\lambda_i^t\}) \right. \\ & \quad \quad \left. - \tilde{\mathcal{L}}(\theta^{t+1}, \{\theta_i^t\}, \{w_i^t\}, \{\lambda_i^t\}) \right) \\ & \quad + \left(\tilde{\mathcal{L}}(\theta^{t+1}, \{\theta_i^{t+1}\}, \{w_i^{t+1}\}, \{\lambda_i^{t+1}\}) \right. \\ & \quad \quad \left. - \tilde{\mathcal{L}}(\theta^{t+1}, \{\theta_i^{t+1}\}, \{w_i^{t+1}\}, \{\lambda_i^t\}) \right). \end{aligned} \quad (17)$$

Each of the three differences on the right-hand side corresponds to the sequential update rule for the variables in Algorithm 1: θ , then θ_i and w_i , and finally λ_i .

Bounding the first term of (17). Note that by the definitions in (15) and (16), $\tilde{\mathcal{L}}_i$ is $(n\rho)$ -strongly convex w.r.t. θ . The averaging step to obtain θ^{t+1} (line 4 of Algorithm 1) is basically performing the minimization of $\tilde{\mathcal{L}}$ w.r.t. θ . In other words, $\theta^t = \arg \min_{\theta} \tilde{\mathcal{L}}(\theta, \{\theta_i^t\}, \{w_i^t\}, \{\lambda_i^t\})$. Therefore,

$$\begin{aligned} & \tilde{\mathcal{L}}(\theta^{t+1}, \{\theta_i^t\}, \{w_i^t\}, \{\lambda_i^t\}) - \tilde{\mathcal{L}}(\theta^t, \{\theta_i^t\}, \{w_i^t\}, \{\lambda_i^t\}) \\ & \leq -\frac{n\rho}{2} \|\theta^{t+1} - \theta^t\|^2. \end{aligned} \quad (18)$$

Bounding the second term of (17). The second difference quantifies the changes in the augmented Lagrangian after updating the local variables θ_i and w_i . Because we perform node sampling, for those edge nodes who are not chosen at each round, their augmented Lagrangian does not change:

$$w_i^{t+1} = w_i \quad \text{and} \quad \theta_i^{t+1} = \theta_i^t, \quad \forall i \notin S_{t+1}. \quad (19)$$

For the chosen node, analyze the change as follows. Since \mathcal{L}_i is assumed to be L -smooth w.r.t. w_i , we have

$$\begin{aligned} & \mathcal{L}_i(\theta_i^t, w_i) \\ & \leq \mathcal{L}_i(\theta_i^t, w_i^t) + \langle \nabla_{w_i} \mathcal{L}_i(\theta_i^t, w_i^t), w_i - w_i^t \rangle + \frac{L}{2} \|w_i - w_i^t\|^2. \end{aligned}$$

By minimizing the right-hand side, we have the GD rule: $w_i^{t+1} = w_i^t - \frac{1}{L} \nabla_{w_i} \mathcal{L}_i(\theta_i^t, w_i^t)$. This leads to the following sufficient decrease to the local loss

$$\mathcal{L}_i(\theta_i^t, w_i^t) - \mathcal{L}_i(\theta_i^t, w_i^{t+1}) \leq -\frac{L}{2} \|w_i^{t+1} - w_i^t\|^2.$$

Since the augmented Lagrangian only differs from the local loss function by a constant w.r.t. w_i , this implies that

$$\begin{aligned} & \tilde{\mathcal{L}}_i(\theta^{t+1}, \theta_i^t, w_i^{t+1}, \lambda_i^t) - \tilde{\mathcal{L}}_i(\theta^{t+1}, \theta_i^t, w_i^t, \lambda_i^t) \\ & \leq -\frac{L}{2} \|w_i^{t+1} - w_i^t\|^2. \end{aligned} \quad (20)$$

To bound the difference but w.r.t. θ_i , note that as per the definition in (15), $\tilde{\mathcal{L}}_i$ is $(L + \rho)$ -smooth w.r.t. θ_i . Using the same logic as above, this time updating θ_i using the gradient of the augmented Lagrangian, we have the following bound

$$\begin{aligned} & \tilde{\mathcal{L}}_i(\theta_i^{t+1}, \theta_i^{t+1}, w_i^{t+1}, \lambda_i^t) - \tilde{\mathcal{L}}_i(\theta_i^{t+1}, \theta_i^t, w_i^{t+1}, \lambda_i^t) \\ & \leq -\frac{L + \rho}{2} \|\theta_i^{t+1} - \theta_i^t\|^2. \end{aligned} \quad (21)$$

Combining (19) to (21), we have $\forall i$,

$$\begin{aligned} & \tilde{\mathcal{L}}_i(\theta_i^{t+1}, \theta_i^{t+1}, w_i^{t+1}, \lambda_i^t) - \tilde{\mathcal{L}}_i(\theta_i^{t+1}, \theta_i^t, w_i^t, \lambda_i^t) \\ & \leq -\frac{L}{2} \|w_i^{t+1} - w_i^t\|^2 - \frac{L + \rho}{2} \|\theta_i^{t+1} - \theta_i^t\|^2. \end{aligned} \quad (22)$$

Bounding the third term of (17). Based on the update of θ_i^{t+1} on line 10 of Algorithm 1, the change in the augmented Lagrangian can be written as

$$\begin{aligned} & \tilde{\mathcal{L}}_i(\theta_i^{t+1}, \theta_i^{t+1}, w_i^{t+1}, \lambda_i^{t+1}) - \tilde{\mathcal{L}}_i(\theta_i^{t+1}, \theta_i^{t+1}, w_i^{t+1}, \lambda_i^t) \\ & = \langle \lambda_i^{t+1} - \lambda_i^t, \theta_i^{t+1} - \theta_i^t \rangle = \frac{1}{\rho} \|\lambda_i^{t+1} - \lambda_i^t\|^2. \end{aligned} \quad (23)$$

Notice that the first-order condition for θ_i^{t+1} implies that

$$\nabla_{\theta_i} \mathcal{L}_i(\theta_i^{t+1}, w_i^{t+1}) + \lambda_i^t + (L + \rho)(\theta_i^{t+1} - \theta_i^t) = 0.$$

Using the fact that $\lambda_i^{t+1} = \lambda_i^t + \rho(\theta_i^{t+1} - \theta_i^t)$, we have

$$\lambda_i^{t+1} = -\nabla_{\theta_i} \mathcal{L}_i(\theta_i^{t+1}, w_i^{t+1}) - L(\theta_i^{t+1} - \theta_i^t). \quad (24)$$

Therefore,

$$\begin{aligned} & \|\lambda_i^{t+1} - \lambda_i^t\| \\ & = \left\| \left[\nabla_{\theta_i} \mathcal{L}_i(\theta_i^{t+1}, w_i^{t+1}) - \nabla_{\theta_i} \mathcal{L}_i(\theta_i^t, w_i^t) \right] \right. \\ & \quad \left. + L[\theta_i^{t+1} - \theta_i^t] + L[\theta_i^t - \theta_i^{t+1}] \right\| \\ & \leq 2 \|\theta_i^{t+1} - \theta_i^t\| + \|w_i^{t+1} - w_i^t\| + \|\theta_i^{t+1} - \theta_i^t\|, \end{aligned}$$

where on the second row, we use the triangle inequality and the fact that \mathcal{L}_i is L -smooth w.r.t. (θ_i, w_i) . This implies that

$$\begin{aligned} & \|\lambda_i^{t+1} - \lambda_i^t\|^2 \leq 12L^2 \|\theta_i^{t+1} - \theta_i^t\|^2 \\ & \quad + 3L^2 \|w_i^{t+1} - w_i^t\|^2 + 3L^2 \|\theta_i^{t+1} - \theta_i^t\|^2. \end{aligned} \quad (25)$$

This result also holds for edge nodes who do not participate in round t , because the left-hand side is simply zero.

Substituting (25) into the right-hand side of (23) gives

$$\begin{aligned} & \tilde{\mathcal{L}}_i(\theta_i^{t+1}, \theta_i^{t+1}, w_i^{t+1}, \lambda_i^{t+1}) - \tilde{\mathcal{L}}_i(\theta_i^{t+1}, \theta_i^{t+1}, w_i^{t+1}, \lambda_i^t) \\ & \leq \frac{12L^2}{\rho} \|\theta_i^{t+1} - \theta_i^t\|^2 + \frac{3L^2}{\rho} \|w_i^{t+1} - w_i^t\|^2 \\ & \quad + \frac{3L^2}{\rho} \|\theta_i^{t+1} - \theta_i^t\|^2. \end{aligned} \quad (26)$$

Combining the differences. Adding together (18), (22) and (26), summing the result over all edge nodes and then the unrolling the result over T global iteration gives

$$\begin{aligned} & \tilde{\mathcal{L}}(\theta^{t+T}, \{\theta_i^{t+T}\}, \{w_i^{t+T}\}, \{\lambda_i^{t+T}\}) - \tilde{\mathcal{L}}(\theta^t, \{\theta_i^t\}, \{w_i^t\}, \{\lambda_i^t\}) \\ & \leq \sum_{k=1}^T \sum_{i=1}^n \left[-\left(\frac{\rho}{2} - \frac{3L^2}{\rho}\right) \|\theta^{t+k+1} - \theta^{t+k}\|^2 \right. \\ & \quad - \left(\frac{L + \rho}{2} - \frac{12L^2}{\rho}\right) \|\theta_i^{t+k+1} - \theta_i^{t+k}\|^2 \\ & \quad \left. - \left(\frac{L}{2} - \frac{3L^2}{\rho}\right) \|w_i^{t+k+1} - w_i^{t+k}\|^2 \right]. \end{aligned} \quad (27)$$

If we choose $\rho > 6L$, then $\left(\frac{\rho}{2} - \frac{3L^2}{\rho}\right)$, $\left(\frac{L + \rho}{2} - \frac{12L^2}{\rho}\right)$ and $\left(\frac{L}{2} - \frac{3L^2}{\rho}\right)$ are all positive. This allows us to move the first sum into each squared norm, we have (13). \square

B. Proof of Lemma IV.5

Proof. For each edge node $i \in S_{t+1}$, we have

$$\begin{aligned} & \tilde{\mathcal{L}}_i(\theta_i^{t+1}, \theta_i^{t+1}, w_i^{t+1}, \lambda_i^{t+1}) \\ & = \mathcal{L}_i(\theta_i^{t+1}, w_i^{t+1}) + \frac{\rho}{2} \|\theta_i^{t+1} - \theta^{t+1}\|^2 + \langle \lambda_i^{t+1}, \theta_i^{t+1} - \theta^{t+1} \rangle \\ & = \mathcal{L}_i(\theta_i^{t+1}, w_i^{t+1}) + \frac{\rho}{2} \|\theta_i^{t+1} - \theta^{t+1}\|^2 \\ & \quad - \langle \nabla_{\theta_i} \mathcal{L}_i(\theta_i^{t+1}, w_i^{t+1}) + L(\theta_i^{t+1} - \theta^{t+1}), \theta_i^{t+1} - \theta^{t+1} \rangle \\ & = \mathcal{L}_i(\theta_i^{t+1}, w_i^{t+1}) + \frac{\rho - 2L}{2} \|\theta_i^{t+1} - \theta^{t+1}\|^2 \\ & \quad + \langle \nabla_{\theta_i} \mathcal{L}_i(\theta_i^{t+1}, w_i^{t+1}), \theta^{t+1} - \theta_i^{t+1} \rangle, \end{aligned} \quad (28)$$

where in the second inequality we substitute expression of λ_i^{t+1} in (24). Now, since \mathcal{L}_i is L -smooth w.r.t. θ_i , we have

$$\begin{aligned} & \mathcal{L}_i(\theta_i^{t+1}, w_i^{t+1}) \\ & \leq \mathcal{L}_i(\theta_i^{t+1}, w_i^{t+1}) + \frac{L}{2} \|\theta_i^{t+1} - \theta^{t+1}\|^2 \\ & \quad + \langle \nabla_{\theta_i} \mathcal{L}_i(\theta_i^{t+1}, w_i^{t+1}), \theta^{t+1} - \theta_i^{t+1} \rangle \\ & = \mathcal{L}_i(\theta_i^{t+1}, w_i^{t+1}) + \frac{L}{2} \|\theta_i^{t+1} - \theta^{t+1}\|^2 \\ & \quad + \langle \nabla_{\theta_i} \mathcal{L}_i(\theta_i^{t+1}, w_i^{t+1}) - \nabla_{\theta_i} \mathcal{L}_i(\theta^{t+1}, w_i^{t+1}), \theta^{t+1} - \theta_i^{t+1} \rangle \\ & \quad + \langle \nabla_{\theta_i} \mathcal{L}_i(\theta^{t+1}, w_i^{t+1}), \theta^{t+1} - \theta_i^{t+1} \rangle \\ & \leq \mathcal{L}_i(\theta_i^{t+1}, w_i^{t+1}) + \frac{3L}{2} \|\theta_i^{t+1} - \theta^{t+1}\|^2 \\ & \quad + \langle \nabla_{\theta_i} \mathcal{L}_i(\theta^{t+1}, w_i^{t+1}), \theta^{t+1} - \theta_i^{t+1} \rangle, \end{aligned} \quad (29)$$

where in the last line we use the Cauchy-Schwarz inequality and again the fact that \mathcal{L}_i is L -smooth. From (28) and (29), we have

$$\begin{aligned} & \tilde{\mathcal{L}}_i(\theta_i^{t+1}, \theta_i^{t+1}, w_i^{t+1}, \lambda_i^{t+1}) \\ & \geq \mathcal{L}_i(\theta_i^{t+1}, w_i^{t+1}) + \frac{\rho - 5L}{2} \|\theta_i^{t+1} - \theta^{t+1}\|^2. \end{aligned} \quad (30)$$

This implies that

$$\begin{aligned} & \tilde{\mathcal{L}}(\theta^{t+1}, \{\theta_i^{t+1}\}, \{w_i^{t+1}\}, \{\lambda_i^{t+1}\}) \\ & \geq \sum_{i=1}^n \left(\mathcal{L}_i(\theta^{t+1}, w_i^{t+1}) + \frac{\rho - 5L}{2} \|\theta_i^{t+1} - \theta^{t+1}\|^2 \right) \\ & = \mathcal{L}(\theta^{t+1}, \{w_i^{t+1}\}) + \frac{\rho - 5L}{2} \sum_{i=1}^n \|\theta_i^{t+1} - \theta^{t+1}\|^2. \end{aligned} \quad (31)$$

Given the assumptions that (i) \mathcal{L} is bounded below by $\underline{\mathcal{L}}$ and (ii) $\rho > 5L$, we establish that $\tilde{\mathcal{L}}(\theta^{t+1}, \theta_i^{t+1}, w_i^{t+1}, \lambda_i^{t+1})$ is lower bounded by $\underline{\mathcal{L}}$. \square

C. Model and Training Details

1) *Model Details*: In this section, we provide details on the models used for the experiment parts. Particularly, the models associated with each dataset are presented as follows.

- **FEMNIST, CIFAR-10, and CIFAR-100**: As for baselines, we employ the convolutional and pooling stages of ResNet-14, ResNet-20, and ResNet-34 [52], each followed by two fully connected (FC) layers for extracting the representation, and an additional FC layer for personalization. For FeDEQ, we introduce DEQ-ResNet models which are designed with a similar structure to ResNet counterparts but utilize a single equilibrium Resnet block design and Softplus activation functions for smoothness objectives. All models, including the specific architectures, the activation functions used, and their respective sizes in megabytes, are detailed in Table V.
- **SHAKESPEARE**: As detailed in Table VI, we design three explicit Transformer-like models based on Universal Transformer [54] for the baselines, featuring 4, 8, and 12 layers respectively. Concurrently, we construct a DEQ-Transformer model for FeDEQ. Each of these models uses an embedding length of 64, and a linear layer with the dimension equal to the vocab size. The Transformer models differ in their number of Universal Transformer (UT) layers and their use of multi-head attention, with the DEQ-Transformer model also employing a similar configuration. The last UT layer and the linear layer are subsequently employed for personalization.

In our experiment setup for personalized tasks, we utilize ResNet-20 for FEMNIST, ResNet-34 for CIFAR-10 and CIFAR-100, and Transformer-8 for the Shakespeare dataset as baseline models. FeDEQ is implemented with DEQ variants of the baseline models. Specific details regarding the shared parameters and personalized parameters, including the number of model parameters and the model sizes, are presented in Table II. From these tables, it's evident that DEQ-ResNet models are 2 – 4 times smaller in size compared to their traditional ResNet counterparts for each corresponding dataset. This suggests that DEQ-ResNet models are more parameter-efficient, providing similar functionality with fewer parameters (see Sec. V). This compactness might lead to less memory consumption and potentially faster computation, which could be beneficial in practical applications, especially where resources are constrained.

D. Training Details

In our research, all experiments are conducted in a coding environment powered by an AMD Ryzen 3970X Processor [55] with 64 cores and 256GB of RAM. Additionally, an NVIDIA GeForce RTX 3090 GPU [56] is to accelerate the training process. For softwares, we rely on Python 3 as our primary language, supplemented by advanced machine learning and optimization frameworks: Jax [57], Haiku [58], Optax [59], Jaxopt [60], and FedJax [51]. Furthermore, our implementation is also inspired by some personalized FL benchmarking works such as Motley [61].

- **FEMNIST**: We employ ResNet-20 as the base model. We use Stochastic Gradient Descent (SGD) as the optimization algorithm, with a learning rate of 0.01. The model is trained using a batch size of 10 across 150 communication rounds.
- **CIFAR-10**: We utilize ResNet-34 as the base model. The model is trained using SGD with a learning rate of 0.01. The training proceeds with a batch size of 20 over 150 communication rounds.
- **CIFAR-100**: We use ResNet-34 for the baseline models and DEQ-ResNet-M for FeDEQ. The learning rate for the baseline models is set at 0.05, while for FeDEQ, it is set at 0.01. The training is conducted with a batch size of 20 across 150 communication rounds.
- **Shakespeare**: We employ Transformer-8 as the base model for baselines, and DEQ-Transformer for FeDEQ. We use SGD with a learning rate of 0.1 for the training process. The model is trained using a batch size of 16 across 400 communication rounds.

These configurations ensure a fair comparison between the baselines and FeDEQ while maintaining a balance between computational efficiency and model performance.

Memory Footprint: To estimate GPU memory usage, we use the system-level *nvidia-smi* command and the *py3nvm* library, which is a Python 3 wrapper around the NVIDIA Management Library. The memory usage is monitoring during the training phases.

E. Additional experiments on the effects of ρ

Here we extend more insights about the effects of ρ on the performance and convergence of FeDEQ. As discussed in Sec. V-B, the parameter ρ in FeDEQ is a tuning parameter that controls the trade-off between the dual constraint satisfaction (i.e., how closely the local representation match the shared representation) and the minimization of the objective function. Therefore, the selection of ρ is crucial for the performance of FeDEQ and it can vary significantly based on the specific optimization problem.

As shown in Fig. 11 and 12, if ρ is too small, the constraint $\theta_i = \theta$ is weakly enforced, meaning that the local variables have more freedom to minimize their local objective function, which might cause the consensus variable to deviate from the optimum. This might increase the number of iterations needed for convergence (e.g., $\rho = 0.001$) or may even prevent convergence in certain cases (e.g., $\rho = 1.0$ in CIFAR-10 and CIFAR-100). On the other hand, it can provide a better local performance as each subproblem can be more optimized

TABLE V: Models employed for FEMNIST, CIFAR-10 and CIFAR-100 Datasets (The model size is shown in megabytes (MB))

Dataset	Model	1 Initial Conv	Residual Blocks		3 FC Layers	Activation Function	Total Model Size
		Output Channel	Blocks/ Group	Output Channels/ Group	Output Dimension		
FEMNIST	ResNet-14	32	(1, 2, 2, 1)	(32, 64, 128, 256)	(256, 128, 62)	ReLU	6.81
	ResNet-20		(2, 3, 2, 2)				11.90
ResNet-34	(3, 4, 5, 3)		20.54				
	DEQ-ResNet-S	64	1 Block with 2 Conv: 64, 128		(256, 128, 62)	Softplus	3.97
CIFAR-10	ResNet-14	64	(2, 2, 2)	(64, 128, 256)	(256, 128, 10)	ReLU	11.34
	ResNet-20		(3, 3, 3)				17.54
ResNet-34	(5, 6, 5)		31.12				
	DEQ-ResNet-M	128	1 Block with 2 Conv: 128, 256		(256, 128, 10)	Softplus	10.91
CIFAR-100	ResNet-14	64	(1, 2, 3)	(64, 128, 256)	(256, 128, 100)	ReLU	15.81
	ResNet-20		(2, 3, 4)				22.01
ResNet-34	(3, 5, 8)		43.56				
	DEQ-ResNet-M	128	1 Block with 2 Conv: 128, 256		(256, 128, 100)	Softplus	10.95

TABLE VI: Models employed for SHAKESPEARE (The model size is shown in megabytes (MB))

Model	Embedding Length	Transformer Block	1 Linear Layer Dimension	Total Model Size
Transformer-4	64	5 UT Layers, 4 Multi-Head Attention	90	1.05
Transformer-8		9 UT Layers, 4 Multi-Head Attention		1.85
Transformer-12		13 UT Layers, 4 Multi-Head Attention		2.45
DEQ-Transformer	64	5 UT Layers, 4 Multi-Head Attention	90	1.05

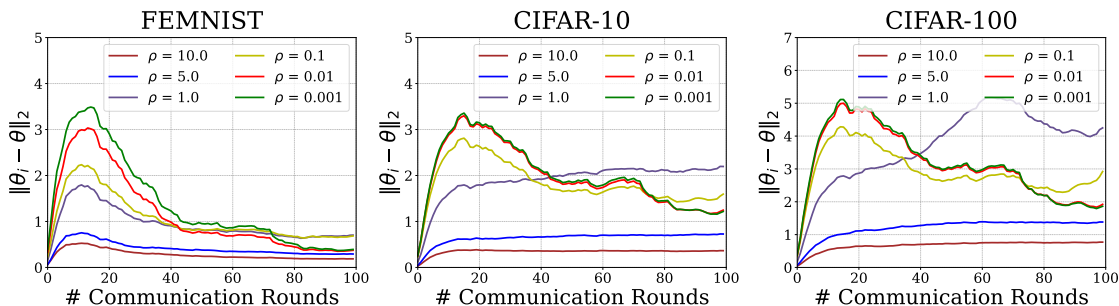


Fig. 11: Effects of ρ on the consensus condition $\theta_i = \theta$ (The residual error $\|\theta_i - \theta\|_2$ are the average L_2 norm of the errors between θ_i for $i = 1, \dots, n$ and θ over iterations)

according to its local data. Conversely, if ρ is too large, the algorithm will strongly enforce the consensus constraint, which can lead to a swift alignment of the local variables to the consensus variable (e.g., $\rho = 5.0$ or $\rho = 10.0$). However, this might cause suboptimal solutions because the strong enforcement of the consensus might prevent local variables from reaching their local optima. In other words, it imposes high "pressure" to force local solutions to agree, potentially at the expense of solution quality. Through empirical evaluation, we found that $\rho = 0.01$ provides the best balance for our datasets. In practice, selecting a suitable ρ often involves trial and error or a validation process. It is also possible to use an adaptive strategy, where ρ is updated during the optimization process.

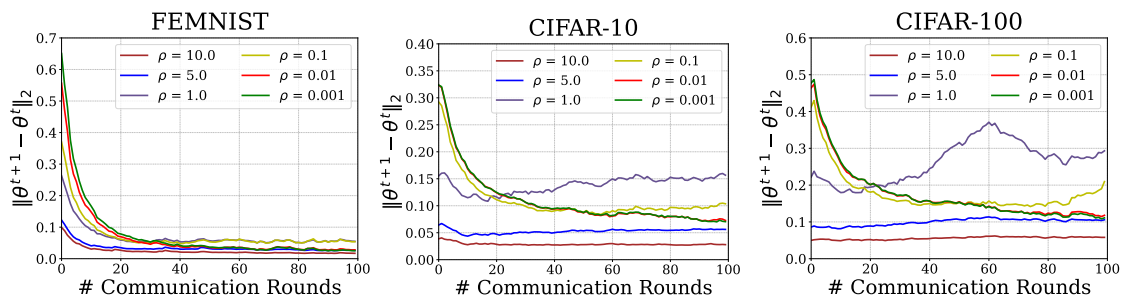


Fig. 12: Effects of ρ on the convergence of the shared representation θ